

University of Windsor

Scholarship at UWindor

Electronic Theses and Dissertations

Theses, Dissertations, and Major Papers

2005

Water and thermal management of PEM fuel cell stack

Xiaochen Yu
University of Windsor

Follow this and additional works at: <https://scholar.uwindsor.ca/etd>

Recommended Citation

Yu, Xiaochen, "Water and thermal management of PEM fuel cell stack" (2005). *Electronic Theses and Dissertations*. 4547.

<https://scholar.uwindsor.ca/etd/4547>

This online database contains the full-text of PhD dissertations and Masters' theses of University of Windsor students from 1954 forward. These documents are made available for personal study and research purposes only, in accordance with the Canadian Copyright Act and the Creative Commons license—CC BY-NC-ND (Attribution, Non-Commercial, No Derivative Works). Under this license, works must always be attributed to the copyright holder (original author), cannot be used for any commercial purposes, and may not be altered. Any other use would require the permission of the copyright holder. Students may inquire about withdrawing their dissertation and/or thesis from this database. For additional inquiries, please contact the repository administrator via email (scholarship@uwindsor.ca) or by telephone at 519-253-3000ext. 3208.

WATER AND THERMAL MANAGEMENT OF PEM FUEL CELL STACK

By

Xiaochen Yu

A Thesis

Submitted to the Faculty of Graduate Studies and Research
through the Department of Mechanical, Automotive and Materials Engineering
in Partial Fulfillment of the Requirements for
the Degree of Master of Applied Science
at the University of Windsor

Windsor, Ontario, Canada
2005

© 2005 Xiaochen Yu



Library and
Archives Canada

Bibliothèque et
Archives Canada

Published Heritage
Branch

Direction du
Patrimoine de l'édition

395 Wellington Street
Ottawa ON K1A 0N4
Canada

395, rue Wellington
Ottawa ON K1A 0N4
Canada

Your file *Votre référence*

ISBN: 0-494-09841-4

Our file *Notre référence*

ISBN: 0-494-09841-4

NOTICE:

The author has granted a non-exclusive license allowing Library and Archives Canada to reproduce, publish, archive, preserve, conserve, communicate to the public by telecommunication or on the Internet, loan, distribute and sell theses worldwide, for commercial or non-commercial purposes, in microform, paper, electronic and/or any other formats.

The author retains copyright ownership and moral rights in this thesis. Neither the thesis nor substantial extracts from it may be printed or otherwise reproduced without the author's permission.

AVIS:

L'auteur a accordé une licence non exclusive permettant à la Bibliothèque et Archives Canada de reproduire, publier, archiver, sauvegarder, conserver, transmettre au public par télécommunication ou par l'Internet, prêter, distribuer et vendre des thèses partout dans le monde, à des fins commerciales ou autres, sur support microforme, papier, électronique et/ou autres formats.

L'auteur conserve la propriété du droit d'auteur et des droits moraux qui protègent cette thèse. Ni la thèse ni des extraits substantiels de celle-ci ne doivent être imprimés ou autrement reproduits sans son autorisation.

In compliance with the Canadian Privacy Act some supporting forms may have been removed from this thesis.

Conformément à la loi canadienne sur la protection de la vie privée, quelques formulaires secondaires ont été enlevés de cette thèse.

While these forms may be included in the document page count, their removal does not represent any loss of content from the thesis.

Bien que ces formulaires aient inclus dans la pagination, il n'y aura aucun contenu manquant.


Canada

ABSTRACT

A water and thermal management model for a Ballard PEM fuel cell stack has been developed to investigate its performance in this thesis. A general calculation methodology has been developed to implement this model. Knowing a set of gas feeding conditions (i.e., pressure, temperature, flow rate) and stack physical conditions (i.e., channel geometry, heat transfer coefficients, operating current), the model will provide information regarding the reaction products (i.e., water and heat), stack power, stack temperature and system efficiency, thereby assisting the designer in achieving the best thermal and water management. Furthermore, if the stack undergoes a perturbation, such as the initial start-up, quick change in current, or a shutdown, the model could predict the dynamic information regarding stack temperature, cell voltage, and power as a function of time.

The issues of two-phase, two-component flow heat transfer and pressure drop along the channel are discussed in this thesis. The performance and efficiency of air compressors and cooling pumps are also considered for the reason of system analysis. By considering all the practical operating parameters mentioned above, this model will provide the optimal stack design pattern and the best working condition, which achieve maximum system efficiency.

ACKNOWLEDGEMENTS

There are lots of people I would like to thank for a variety of reasons.

I would like to express my appreciation of Dr. Biao Zhou for providing me this opportunity of Master degree study, and thank him for his supervision and support within these two years.

Also, I would like to thank Dr. Chunhong Chen, Dr. Andrzej Sobiesiak, Dr. William Altenhof who gave so much useful advice on my graduation proposal and thesis. Special thanks also go to Dr. Andrzej Sobiesiak for providing invaluable support of fuel cell stack testing, and I must say a thank you to Dr. David Ting to be the chair of my defense.

I would like to thank my colleagues in our team: Yi Zong, Wenbo Huang and Peng Quan, for their helpful advices, enduring support and cooperation, as one member of it, I'm proud of our group.

In addition, I must give special thanks to my friend Chengwu Li, for his selfless friendship and help during the 18 years, also best wishes to his families.

This work was supported by the Auto21 Networks of Centres of Excellence Grant D07-DFC.

TABLE OF CONTENTS

ABSTRACT	III
ACKNOWLEDGEMENTS	IIIV
LIST OF FIGURES	VIII
LIST OF TABLES	IX
NOMENCLATURE	X
1. INTRODUCTION	
1.1 PEM FUEL CELL WORKING PRINCIPLE	1
1.2 PEM FUEL CELL STACK AND SYSTEM	4
1.3 OPERATING PARAMETERS MANAGEMENT	12
2. LITERATURE REVIEW AND MOTIVATIONS	
2.1 LITERATURE REVIEW	13
2.2 MOTIVATION	15
3. MATHEMATICAL MODEL	
3.1 BASIC ASSUMPTION	18
3.2 STEADY-STATE ELECTROCHEMICAL MODEL	19
3.3 STEADY-STATE THERMAL MODEL	21
3.4 TRANSIENT MODEL	28
3.5 PRESSURE DROP	29
3.6 WATER TRANSFER ACROSS MEMBRANE.....	31
3.7 CALCULATION OF AIR COMPRESSOR	33
3.8 CALCULATION OF COOLING PUMP	36
3.9 CALCULATION CASE AND PUMP CHARACTERISTIC CURVE.....	37
4. TWO-PHASE FLOW STUDY IN CATHODE CHANNEL	
4.1 GENERAL INTRODUCTION.....	39
4.2 FLOW REGIME IN CATHODE CHANNEL	41
4.3 HEAT TRANSFER CALCULATION/CORRELATION	48
4.4 PRESSURE DROP CALCULATION/CORRELATION.....	49
5. SOLUTION METHODOLOGY	
5.1 ALGORITHM AND THE INTERACTION AMONG THE MODELS.....	51
5.2 STEADY STATE MODELS	54
5.3 UNSTEADY STATE MODELS	55
6. RESULTS AND DISCUSSIONS	
6.1 VALIDATION OF THE MODEL.....	57
6.2 STEAY CASES	59
6.3 STEADY CASES WITH DIFFERENT ϕ VALUE AT INLET	61
6.4 UNSTEADY CASES	63

6.5	WATER TRANSPORTATION	69
6.6	SYSTEM VIEW OF EFFICIENCY	71
7.	CONCLUSIONS AND RECOMMENDATION.....	74
	REFERENCES.....	76
	VITA AUCTORIS	82

LIST OF FIGURES

Fig. 1A. Stack 3-D structure	1
Fig. 1B. Single cell 2-D structure	2
Fig. 2. Curve of voltage loss vs inlet pressure [39]	6
Fig. 3. Roots compressor	8
Fig. 4. Screw compressor.....	9
Fig. 5. Centrifugal compressor.....	10
Fig. 6. Axial type compressor.....	10
Fig. 7. Fuel cell water pump	12
Fig. 8. Schematic of streams parameters and energy terms.....	21
Fig. 9. Pump for coolant	36
Fig. 10. Pump characteristic curve under different flow rates and pressures	38
Fig. 11. Flow regime map from [40].....	44
Fig. 12. Flow regime inside cathode channel [41].....	45
Fig. 13. Film-thickness distribution around circumference of the pipe [42]	46
Fig. 14. Interaction between different models	53
Fig. 15. Steady Case calculation methodology.....	54
Fig. 16. Unsteady case calculation methodology.....	55
Fig. 17. Exit temperatures of flow streams with currents from 2 to 80A	60
Fig. 18. Stack power output with steady operating current from 2 to 80A.....	60
Fig. 19. Anode exit temperature at $\phi_{a,in}=0.5, 1.0$ and 1.5	61
Fig. 20. Stack temperature and voltage at current from 2 to 80 A.....	62
Fig. 21. Stack voltage with different $\phi_{a,in}$ at steady current from 2 to 80A	63

Fig. 22. Transient exit temperature plots of the start-up process for the operating current at 30A	64
Fig. 23. Transient plot of the stack temperature and voltage of the start-up process for the operating current at 30A.....	64
Fig. 24. Transient plot of exit temperature of flow streams during the load set-up from 30-50A.....	65
Fig. 25. Transient plot of stack parameters during the load set-up from 30 to 50 A	66
Fig. 26. Exit temperature change with time/load ($\phi_{a,in} = \phi_{c,in} = 1.0$)	67
Fig. 27. Stack temperature and voltage change($\phi_{a,in} = \phi_{c,in} = 1.0$).....	67
Fig. 28. Stack voltage as a function of current which changes with time as $I = 50 + 20 \sin(t\pi/30)$	68
Fig. 29. Stack power output and efficiency as a function of current of which changes with time as $I = 50 + 20 \sin(t\pi/30)$	69
Fig. 30. Water transfer amount at the operating current from 2 to 80A	70
Fig. 31. Stack efficiency and anode average RH, exit RH at the operating current from 2 to 80A	70
Fig. 32. Efficiency of fuel cell stack and the system at different operating pressure ($I = 20A, \phi_{a,in} = 1.0$)	71
Fig. 33. Power consumed and stack generated under different operating pressure ($I = 20A$)	72
Fig. 34. Efficiency of fuel cell stack and the system at different operating pressure ($I = 20A, \phi_{a,in} = 1.5$)	73

LIST OF TABLES

Table 1	Cathode channel flow data	42
Table 2	Dimensionless parameters for flow regime	43
Table 3	Heat transfer coefficients chart.....	48
Table 4	Inlet parameters of stack Ballard Mark V at 20A	57
Table 3	Stack and channels dimension table.....	57
Table 6	Result comparison with the experimental data ($\phi_{a,in} = \phi_{c,in} = 1.0$).	59

NOMENCLATURE

a	water activity
A	area, m^2
c	water concentration in the membrane, mol m^{-3}
C_p	average heat capacity, $\text{J kg}^{-1} \text{K}^{-1}$
d	channel height, m
D_m	water diffusion coefficient, $\text{m}^2 \text{s}^{-1}$
E	thermodynamic potential, V
f	fraction coefficient of channel
F	Faraday's constant, $F = 96485$
Fr	Froude number
h	convective heat transfer coefficient, $\text{W m}^{-2} \text{K}^{-1}$
H	change in enthalpy, J mol^{-1}
L	channel length, m
i	operating current, A
I	current density, A cm^{-2}
I_0	exchange current density, A cm^{-2}
K	thermal conductivity, $\text{W s}^{-1} \text{m}^{-1} \text{K}^{-1}$
k_p	water hydraulic permeability in membrane, $\text{m}^2 \text{s}^{-1}$
\dot{m}	fluid mass flow rate, kg s^{-1}
M	mass of the fuel cell, kg
n	number of cells in the stack

N	molar flow rate, mol s ⁻¹ ; channel number
n_d	electro-osmotic drag coefficient
n_e	mole number of electrons per unit current per unit time
p	pressure, atm
P	power output, W
PEM	proton exchange membrane
q	heat transfer rate, W
R	universal gas constant; 8.314 J mol ⁻¹ K ⁻¹
Re	Reynolds number
RH	relative humidity
SH	stack height, m
SW	stack width, m
T	temperature, K
t	thickness, m
V	output voltage, V; velocity, m s ⁻¹
x_i	mole fraction of species i
\dot{W}	power

Greek letters

α	excess coefficient
ΔH	heat of reaction, J mol ⁻¹
η	overvoltage, V
ϕ	relative water content
λ	water content of membrane

μ water viscosity, Pa s
 δ membrane conductivity, $\Omega^{-1}\text{m}^{-1}$

Subscripts

0 standard condition
a anode
act activation
c cathode
cell proton exchange membrane fuel cell
cons consumed
conv convection flux
diff diffusion flux
elec electrical
g gas
hum humidification
in in
inlet flow inlet stack channel
int internal
l liquid
loss loss
m membrane
mass mass transfer and/or mass consumption
ohmic ohmic

<i>out</i>	out
<i>outlet</i>	flow outlet stack channel
<i>prod</i>	product
<i>room</i>	ambient condition
<i>rxn</i>	reaction
<i>stack</i>	fuel cell stack
<i>sens</i>	sensible
<i>theo</i>	theoretical
<i>trans</i>	water transfer across membrane
<i>w</i>	water

Superscripts

<i>avg</i>	average value
<i>channel</i>	stack flow channel
<i>dry</i>	dry gas condition
<i>new</i>	current value in iterative calculation
<i>old</i>	previous value in iterative calculation
<i>s</i>	superficial
<i>sat</i>	saturation condition
*	at the catalyst interface

1. INTRODUCTION

In this chapter we will introduce the basic working principle of the PEM fuel cell, how the PEM fuel cell stack works, what the major concerns are in fuel cell system set up, and the optimization of stack operation.

1.1 PEM fuel cell working principle

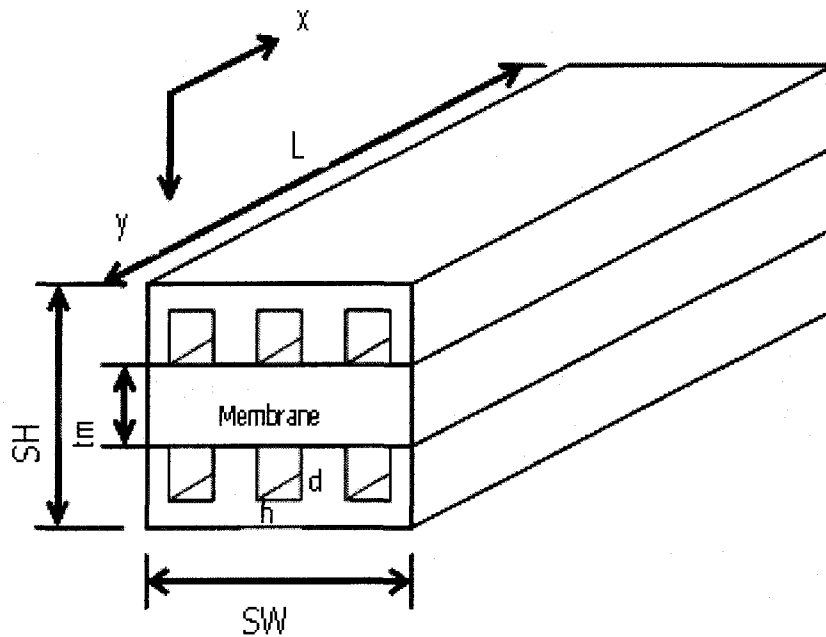


Fig. 1a. Stack 3-D structure

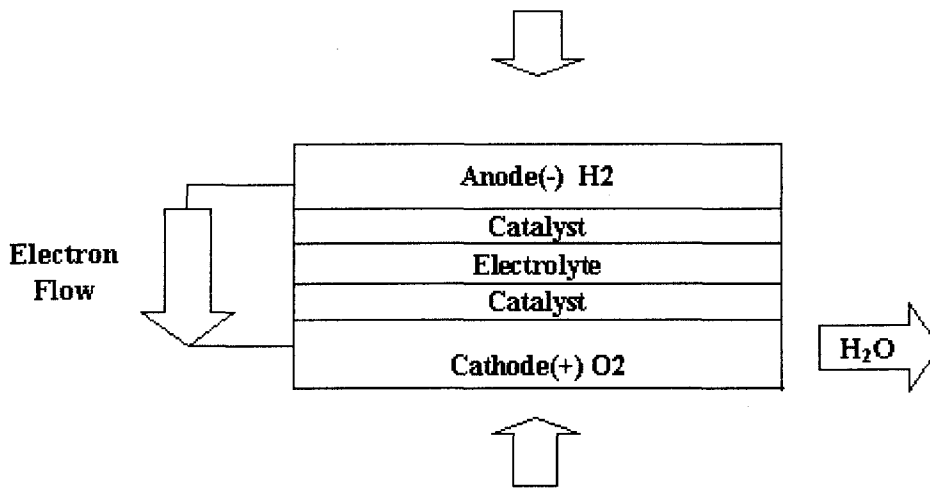


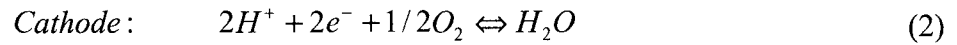
Fig. 1b. Single cell 2-D structure

The above two figures explain how the fuel cell works. These figures show the structure of one single PEM cell, but don't represent the real dimension. Each cell consists of one anode and one cathode. In the middle, a single solid membrane works as the electrolyte. Both surfaces of membrane are coated with catalyst particles in order to increase the chemical reaction speed. When hydrogen gas is fed through the anode, it will run into the fuel cell along the anode channel. Once they reach the anode side of the membrane catalyst layer, the hydrogen ionizes, releasing electrons, and creating H^+ ions. Without a catalyst, this reaction will only occur at higher temperatures. This is why the PEM fuel cell can run at lower temperature.

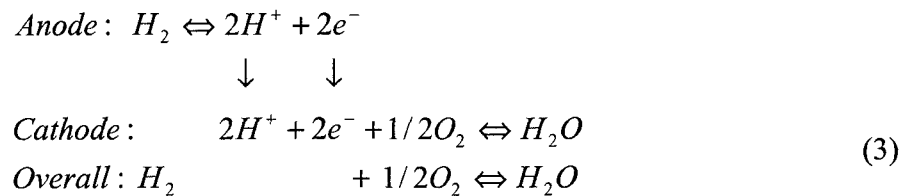


After hydrogen break down, only hydrogen ions can pass through solid membrane, and so the electrons must use the external circuit to reach the cathode side. This type of fuel cell is called a Proton Exchange Membrane (or PEM) because the solid membrane is

electrical insulator. On cathode side, arrived hydrogen ions and electrons will meet the feeding air which comes from cathode channel together to form water and release heat.



Overall view of this device, when we continue feed hydrogen and air, there will have a stable electrical current from anode to cathode via the external circuit. Water appears in the cathode channel, and reaction heat will increase the temperature of both streams and solid.



The potentials formed by anode hydrogen ions and cathode electrons will output as the cell voltage, and in general this voltage is around 0.6~0.7 volts for per cell. Because each single cell's output power is limited, a bank of cells will be assembled serially in real application in order to achieve higher power output and current collector will make a conducting bridge between the cells. Depend on the number of cells, and the active area of each cell, the total stack power can be in the range of several watts to hundreds kilowatts. PEM fuel cells have excellent start up and turndown abilities, it is a quiet device due to the fact there are no moving parts. They have zero emissions which makes it an environmentally friendly source of energy. Finally solid electrolytes make it corrosion and leakage free. All these advantages make PEM fuel cells a promising technology in transportation industry.

1.2 Fuel cell stack and system

In all applications of fuel cells, whether an on board engine, stationary power plant or in a CHP system, there are some main components in the system. We will give a brief introduction here.

A subsystem that needs to be mentioned is the fuelling/air system. PEM fuel cells must use pure hydrogen gas as the fuel, which is obtained from anything from some fossil fuels such as petroleum or natural gas to coal or bio-fuels such as methanol and ethanol. Before these raw primary fuels are supplied to the stack, fuel reforming and processing is the essential method to guarantee that the feeding gas meet the particular stack fuel requirement. For example, a PEM stack needs to be carbon monoxide free, and must have a very low level of sulphur. The most common reforming methods include steam reforming, partial oxidation reforming (POX), catalyst partial oxidation reforming (CPOX) and auto thermal reforming (ATR). In this thesis, we don't go into fuel reforming. Our system model will not include the reformer part. It is assumed that the hydrogen is provided, possibly from a high pressure container.

The air is introduced into the stack at certain pressure by a compressor. High inlet pressure will increase the oxygen partial pressure on the catalyst layer, and will speed up the chemical reaction which achieves higher cell output voltage. However a higher compression ratio will also cause lower compressor efficiency by consuming more electrical power. From the system view to air supply, the optimization condition must be reached under one calculated stack cathode inlet pressure after one type of compressor is selected.

The cooling system is another important component of fuel cell system. Usually a PEM fuel cell stack has an optimal operating temperature range, and this range will vary with different inlet parameters such as mass flow rate, humidification rate, reactant pressures and even the dimensions of the channel. Low stack temperature will cause a slow electrochemical reaction, as a result, the stack output voltage will be reduced. Increased stack temperature does speed up the reaction and reduce activation loss, however there are negative effects. At first it will enhance the partial pressure of water vapour inside the channel. For an inlet pressure fixed channel, it will reduce the partial pressure of the reactants. Secondly, as we know, the gas humidification rate is sensitive to temperature, so if the total water amount inside the channel is fixed, higher temperature will reduce the relative humidification rate of the reactants (especially on the anode side). Lower humidification rate will cause the membrane to dry, which has negative effects on membrane conductivity. So for temperature issue, we need a dynamic analysis to find out the best solution to the system parameters. We will discuss the cooling effect in Chapter 6. Model Validation and Results Analysis by comparing the result of water cooling under different operating conditions.

1.2.1 Water pump and air compressor

Hydrogen and air are introduced into the fuel cell channels at high pressure, and compressor will be used to increase the inlet fuel /air pressure. For cooling system, the coolants will be driven by water pump or air blower for cooling circulation. These pump, blower and compressor will consume the electrical power generated by fuel cell stack. From the view of system optimization, proper select and define working conditions of these auxiliary equipments will be very important to system efficiency, all these are

considered into our model calculation. In the next subsection, the brief summary is given for a better understanding about this. The hydrogen gas is fed to the anode channel from pressurized container or fuel reformer, before hydrogen gas run into stack, the high pressure gas provide by container or reformer must go through regulator to reach the designed inlet pressure value of anode, it is called “comes free”, because no stack power will be consumed. Based on this reason, we don’t consider anode side gas compressor here, if necessary, we can treat it the same way as we do below for cathode channel.

1.2.2 Cathode air compressor

Most of larger fuel cells are operated at higher pressures. The purpose of increasing the operating pressure is to increase stack power output while the other parameters keep the same, because higher pressure will raise the exchanger current density, reduce cathode side activation loss. We can observe this from the Equation (5) and the Fig. 2 from [39].

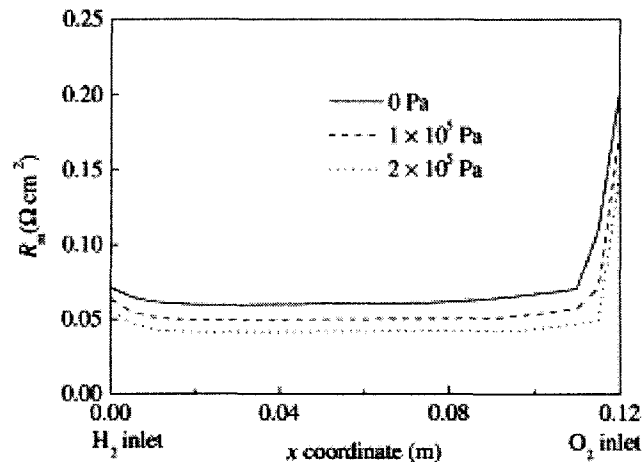


Fig.2. Curve of voltage loss vs inlet pressure [39]

But increasing inlet air pressure will cause extra burden on extra compressor space, weight, it is impossible if the stack has a strict volume limitation. Furthermore, the air compressor is driven by an electrical motor, which uses up more of the limited electricity generated by the stack itself. In general, the compressor will consume up to 20% of the stack power, so the trade off between higher and lower operating pressure are complex, this must be considered on both sides in order to achieve the optimized operating condition.

The types of compressors used in fuel cell systems are the same as those used in other industrial applications. The only restriction is that the use of output compressed gas and lubrication oil is not acceptable, it will contaminate the fuel cell catalyst. The four main types air compressor are roots compressor, screw compressor, centrifugal compressor and axial flow compressor. Different types of compressors will be used in different working conditions. Here we give a brief introduction on how to select correct types of compressors.

The Roots compressor consists of two rotor wheels each with two or three lobes. The roots type is known for its ability to produce large amounts of boost while spinning at very low speeds. Another advantageous characteristic of the roots type compressor is its simplicity of design. The roots type has very few moving parts and spins at low RPMs, making it one of the more reliable and durable designs. Roots compressor is quite cheap and easy for manufacturing, and has a wide range of operating flow rates. But when the pressure compression ratio is higher, it will provide lower efficiency, heavy internal parts mean high parasitic losses when boosting. So in general case, root type only be considered when the compression ratio is lower than 1.3~1.4. Another big disadvantage

to the roots type is its thermal inefficiency, the poor thermal efficiency can be attributed to the fact that it has no internal compression (compression is done after the air leaves the discharge port). Additional heat is created by compressed (hot) air that leaks backwards past the rotors and heats up the temperature of the inlet charge. The large size and difficulty of placement also can make it hard to add an intercooler.

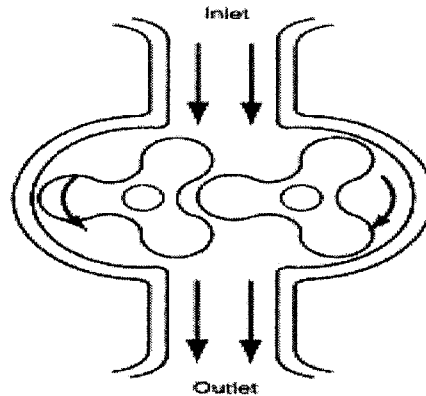


Fig. 3. Roots compressor [48]

Screw compressors have proven to be the most cost efficient choice for low pressure and wellhead compression applications. The unique ability to load horsepower over a wide range of operating conditions give the rotary screw a huge advantage over other methods of compression. Screw compressors have the familiar two rotors, twisted lobe design provides higher efficiency at a wide range of compression ratio and flow rates, the compression ratio can be up to 8. Advantages of the rotary screw compressor include smooth, low noise levels and pulse-free air output in a compact size with high output volume over a long life. The disadvantage is they are expensive to manufacture for the high rotor precision.

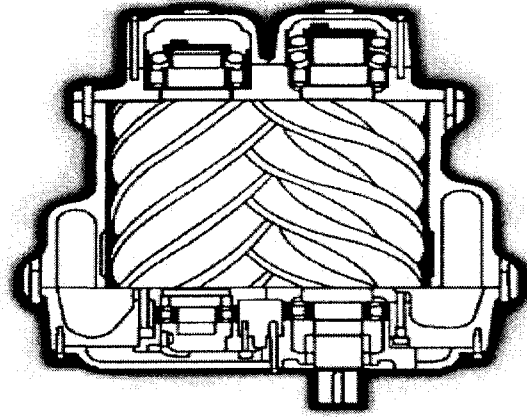


Fig. 4. Screw compressor [49]

Centrifugal compressors are the most common dynamic compressors with the advantages of low cost and easy to manufacture, which raise the pressure of air by imparting velocity energy, the flow through the compressor is turned perpendicular to the axis of rotation. These compressors work done by using a veined wheel, which spins inside a specially designed housing, using a rotating impeller, and converting it to pressure energy. Centrifugal compressors are oil-free by design, the oil lubricated running gear is separated from the air by shaft seals and atmospheric vents to keep compressed air clean. They have few moving parts hence decreasing maintenance requirements and costs. Centrifugal compressors are designed to handle a base or continuous load in compressed air systems because they have limited turn-down or reduced output capability. It only works at reasonable efficiencies with quite defined flow rates and compression ratio, during the load variability over time, the efficiency will not be acceptable. When the flow rate is very low, the performance is even worse. High compressor RPM means lower long term reliability, the internal tolerances must be very exacting, furthermore, the bearing of high speed rotor need to be lubricated.

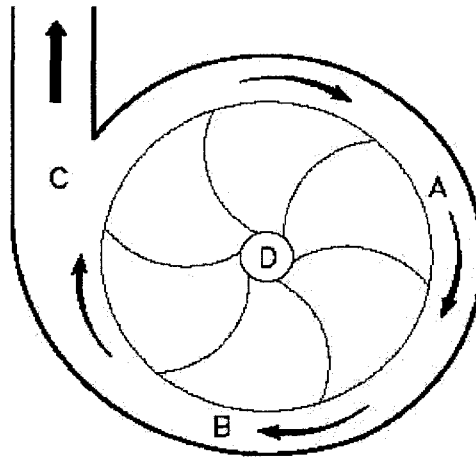


Fig. 5. Centrifugal compressor [50]

In the axial compressor, the air flows parallel to the axis of rotation. The compressor is composed of several rows of airfoil cascades. Some of the rows, called rotors, are connected to the central shaft and rotate at high speed. Other rows, called stators, are fixed and do not rotate. The job of the stators is to increase pressure and keep the flow from spiraling around the axis by bringing the flow back parallel to the axis. Axial flow compressors are expensive to manufacture and has a narrow range of high efficiency flow rates, only considered under the fixed working conditions.

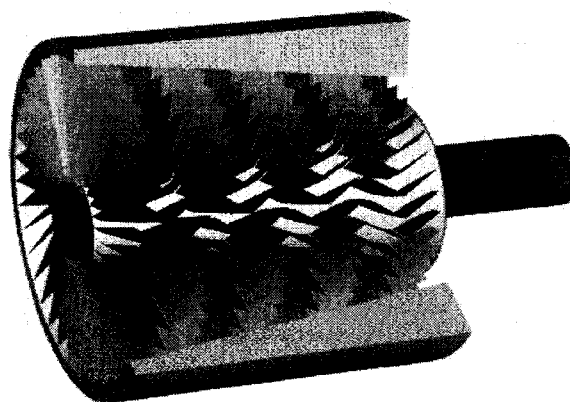


Fig. 6. Axial type compressor [51]

For the compressor selection, it is very important that the designer couldn't select a compressor simply by using the max mass flow rate, ignore both the compression ratio ranges and the flow rate range. Budget consideration and design around what is actually available from the current products are also the key point. The turn down abilities will be another issue of selection. Basically the rules are for higher compression ratio case, the screw type is the first choice for the reason of flexibility and efficiency; For smaller size stack, it is difficult to obtain a suitable compressor, consider centrifugal type if the flow rate range is narrow; And there is a wide range of available products when stack power is over 50kw, avoid employ centrifugal compressor if there is a flexible flow change during the operation.

1.2.4 Cooling system

During the stack operation, for a fixed inlet gas pressure, stack solid temperature must be in a certain range in order to achieve higher performance. The cooling system is divided into two catalogues by the coolant, air cooling and water cooling. In general, air cooling is considered only at small size stack operation for the reason of compact, simple power efficient, easy to maintain and no leakage or channel block happen, the weakness of air cooling is its limited cooling capacity and turn down variability. Water cooling will have higher requirements for the coolant channel design and the assembly of sealing, also the cooling system will increase stack volume, the trade off is a better cooling effect and flexibility when dealing with different operating conditions, also the coolant water with higher temperature can be the heating source of a CHP system. We consider water cooling in this thesis only. At different operating conditions, circulating water will be introduced by water pump at different flow rates. The size range of current available

water pump in fuel cell application is from 10gpm to over 500gpm (Steward Division Company index)

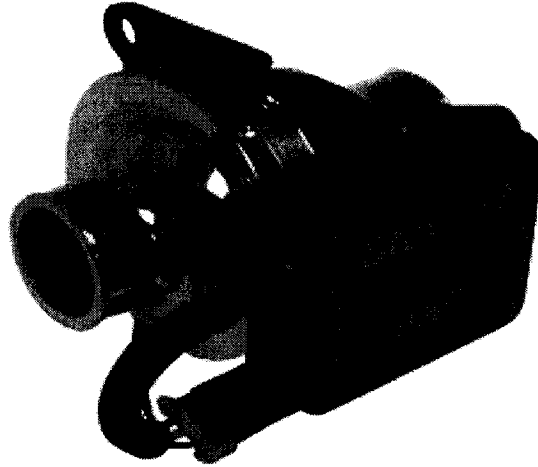


Fig. 7. Fuel cell water pump [52]

1.3 Operating parameters management

When the fuel cell stack/system is running under one specific working condition, the parameters like flow rate, pressure, temperature must be in a reasonable range to achieve the best system efficiency. Based on the model we have set up, we will know how the change of each parameter will affect the stack output parameters, and the interaction among the models. These are the necessary data needed of water and thermal management.

2. LITERATURE REVIEW AND MOTIVATIONS

2.1 Literature review

A proton exchange membrane (PEM) fuel cell is an electrochemical device where the energy of a chemical reaction is converted directly into electricity, by combining hydrogen fuel with oxygen from air [1]. Water and heat are the only by-products if hydrogen is used as the fuel source for PEM fuel cell. Most of the current research and development efforts focus on PEM fuel cells due to their capability of higher power density and faster start-up than other fuel cells [2-6]. Usually PEM fuel cells could be operated at a temperature lower than 100°C, thus faster start-up and immediate response to changes in the demand for power could be realized.

Water and thermal management has become one of the key technical challenges that must be resolved in order for the PEM fuel cell technology to be feasible for transportation applications [7, 8], although, over the last decade, significant progress has been made in the field of PEM fuel cell stack development [9-11]. Proper water and thermal management is essential for optimizing the performance of a fuel cell stack.

In automotive applications, there are many different road conditions and events involved and therefore the knowledge on the PEM fuel cell stack in terms of steady and transient behaviour (e.g., acceleration, deceleration) becomes very important. In an automotive fuel cell stack, water and thermal management on this steady and transient behaviour is associated with many parameters that affect the design and performance of PEM fuel cell. In order to understand the relative importance of the parameters and their interaction, an investigation of these parameters is required [12]. Mathematical modeling,

a convenient and powerful tool, is therefore well suited for this task. The numerical modeling could be employed to significantly reduce the time and cost associated with the PEM fuel cell stack development.

To date, most of the work done in terms of PEM fuel cell modeling has focused on the electrochemical and diffusion processes of individual fuel cells (also called a unit cell). Some noteworthy early examples include Dunbar and Gaggioli [13], Springer and Zawodzinski [14], Verbrugge and Hill [15], Bernardi and Verbrugge [16, 17], Fuller and Newman [18], Ngyyen and White [19] and Kim et al.[20]. University of Victoria and University of Waterloo [21-25] have been conducting the fuel cell modeling for many years and have made very impressive progress on the unit cell modeling.

The models mentioned above mainly emphasized on understanding and improving the kinetic processes that occurred in fuel cell, aiming at improving individual fuel cell performance. The researchers built their models based on electrochemical theories, electrode kinetics and experimental data.

As mentioned by Costamagna and Srinivasan [26], until the year 2000, no detailed results of the modeling analyses of the performance characteristics of the electrochemical cell stack and the PEMFC power plant had appeared in the literature. Models of fuel cell stacks have been and are being conducted by some fuel cell companies and such development remains in proprietary.

Texas A&M University [27, 28] made very good contribution to the fuel cell stack modeling. However, their model only focused on fuel cell stack and the model did not consider two-phase flow and liquid water was not considered. In real fuel cell processes,

both liquid water and vapour are very important factors that have to be resolved properly in order to have stable fuel cell operation.

Some thermal models of PEM fuel cell stacks could be found in the literature [29-32]. These models typically treat the stack as a process unit and develop models based on electrochemical performance, and the physical characteristics of the inlet and outlet flows. The computations of these models are usually too involved to be employed in a comprehensive model of a PEM fuel cell stack. A need exists for a technique that can be used to determine the PEM fuel cell stack thermal performance without requiring a significant amount of computations. Some excellent studies on these topics have been conducted by a group of scientists in Royal Military College of Canada [33-36]. In [37] by Yu and Zhou, an improved model was built to consider the inlet water vapour effects.

To our knowledge, the models mentioned above have not included the liquid water effects in the calculation, especially the inlet water (liquid and vapour) effects that could play a very important role in the PEM fuel cell performance. Therefore, in this thesis study, a two-phase model with phase change was built to meet this challenge.

2.2 Motivations

When we review the literature on fuel cell research, we find that the previous works on fuel cell modeling and thermodynamic calculation have some certain limitations. Most of them have separated thermal model and electro-chemical model, i.e., they either use assumed fixed thermal data such as stack temperature in electro-chemical calculation or use a fixed electro-chemical data in their thermal model. However, as we know, these two models interact with each other; affect each other in the real operation, with the

status change of one model, there must be a dynamic response in another, model separation will bring an unfeasible result. So set up a combined thermal and electro-chemical model is our first motivation.

No previous work considers the water management issue in a thermal and electro-chemical combined model, although in fact, water content is a vital issue to stack performance in both stages of vapour and liquid. The model without water management can not reflect stack comprehensive thermal-electrical characteristics in real application. Based on this, we do consider the water amount influence in our combined model in membrane conductivity and channel heat transfer fields.

In order to make our simulations more accurate, our model covers the topics of pressure drop and heat transfer calculation for different channel designs patterns; air and water cooling effects comparison. For the purpose of operating optimization analysis, water pump and air compressor are also involved into our dynamic simulations for system efficiency calculation when dealing with different flow rates.

Another important motivation is to develop one fuel cell simulation/calculation tool based on the thermodynamic and electrochemical models which can be used in a wide operating range to provide useful information for fuel cell design. For fuel cell designers, when they design fuel cell system, they want to predict the system performance (i.e., stack power output, system efficiency) after the inlet condition is defined, or they want to optimize their design pattern to achieve highest system efficiency by changing inlet parameters. Instead of a serial experimental test, a powerful calculation/simulation tool is required to determine PEM fuel cell stack power and thermal performance without

requiring a significant amount of computations. By this way, the period from system modeling and concept design to prototype will be greatly reduced. This simulation will also be used in fuel cell product development by optimal condition integration after finding out the influent of key parameters.

In order to enhance the correctness and generality of our model, based on [37] by X. Yu and B. Zhou, an improved model will be implemented to meet our desired goals by considering:

- (1) The inlet water/vapour effects.
- (2) Water transportation across membrane.
- (3) Cathode side two-phase flow heat transfer.
- (4) Pressure drop and channel geometry effects.

Under these considerations, this improved sophisticated model can be used in a wide range of fuel cell simulation.

3. MATHEMATICAL MODEL

In this chapter, the model will be introduced from the aspects of a thermal model, electro-chemical model, water management model and transient model. Also, the issues of pressure drop, water amount of each phase calculation and the transfer amount across membrane are discussed here.

3.1 Basic assumption

For modeling purposes, the following assumptions were made in the present study:

- (1) Ideal gas law is employed for gaseous species.
- (2) The product water generated at the cathode is assumed to be in liquid state.
- (3) The liquid water was assumed to exist at the surface of the channels, and the volume to be negligible.
- (4) The water condensation/evaporation rate is not considered. Instead, the equilibrium between the water vapour and liquid is always assumed.
- (5) Stack temperature is uniform due to high thermal conductivity.
- (6) Water transport in and out of the electrodes was in the form of vapour.
- (7) The electrode layers were “ultra-thin”, so that gas transport resistance through the electrode porous layer could be neglected.

(8) The entrance and exit losses were neglected, which were too small compared with the overall pressure drop.

In order to describe both cases either with or without phase-change, parameter ϕ , relative water content, was defined as follows:

$$\phi = \frac{\text{Total mole number of water (vapor + liquid)}}{\text{Maximum possible mole number of water vapor}} \quad (4)$$

According assumption (4), when $\phi \leq 1$, it is exactly the same as relative humidity and there is no liquid water; while $\phi > 1$ means there is liquid water and ϕ is no longer equivalent to the relative humidity.

3.2 Steady-State Electrochemical Model

The steady-state electrochemical model could be used to predict stack voltage output. The cell voltage was defined in terms of the following three terms [33]: the thermodynamic potential E , the activation over-voltage η_{act} , and the ohmic over-voltage η_{ohmic} .

$$V_{cell} = E - \eta_{act} - \eta_{ohmic} \quad (5)$$

where

$$E = 1.229 - 0.85 \times 10^{-3} \times (T_{stack} - 29815) + 4.3085 \times 10^{-5} \times T_{stack} \times [\ln(p_{H_2}^*) + 0.5 \times \ln(p_{O_2}^*)] \quad (6)$$

Here by considering the pressure drop from friction effect and concentration decline from reactant consumption, the partial pressure was introduced by averaging the inlet and outlet partial pressures [34]:

$$P_{H_2}^{avg} = \frac{1}{2}(P_{H_2,in} + P_{H_2,out}) \quad (7)$$

$$P_{O_2}^{avg} = \frac{(P_{O_2,in} + P_{O_2,out})}{\ln \frac{P_{O_2,in}}{P_{O_2,out}}} \quad (8)$$

The effective partial pressure of hydrogen and oxygen on catalyst layer now can be calculated to modify the original model by using the averaged partial pressure [34]:

$$P_{O_2}^* = P^{avg} \left[1 - x_{H_2O}^{avg} - x_{N_2}^{avg} \exp\left(\frac{0.291 I}{T_{stack}^{0.832}}\right) \right] \quad (9)$$

$$P_{H_2}^* = P^{avg} \left[1 - 0.5 x_{H_2O}^{avg} - x_{CO_2}^{avg} \exp\left(\frac{0.183 I}{T_{stack}^{0.832}}\right) \right] \quad (10)$$

The activation overpotential and ohmic overpotential could be calculated as follows [19]:

$$\eta_{act} = \frac{R(273.15 + T_{stack})}{0.5 F} \ln \left(\frac{I}{I_0 P_{O_2}} \right) \quad (11)$$

$$\eta_{ohmic} = \frac{I t_m}{\sigma_m} \quad (12)$$

where T_{stack} is the stack temperature (K), I is the operating current (A), I_0 is the exchange current, p^* is the partial pressure on the catalyst interfaces corresponding to concentration of feeding gas, t_m is the membrane thickness and δ_m is the membrane conductivity. The calculation equation of δ_m will be given in water management model section.

3.3 Steady-State Thermal Model

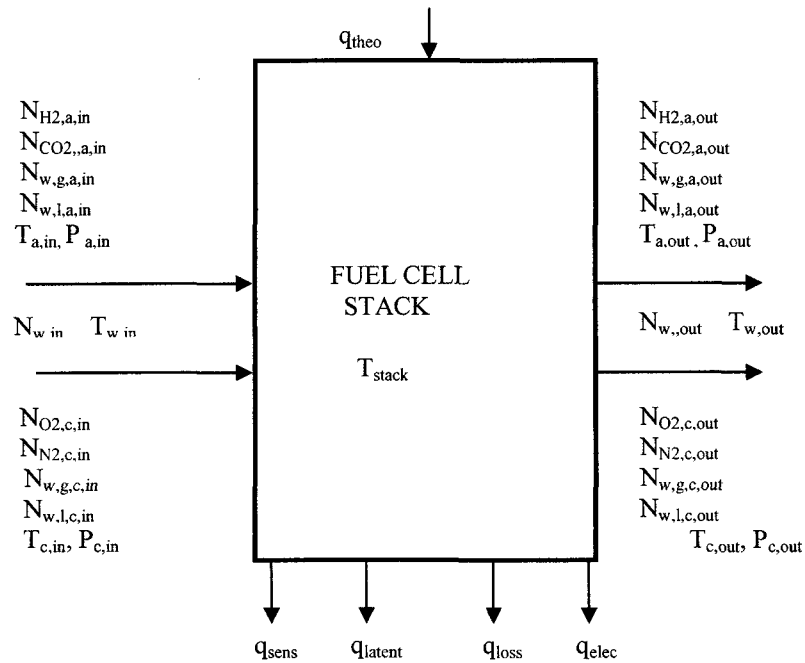


Fig. 8. Schematic of streams parameters and energy terms.

A steady-state thermal model was established based on the balance of mass and energy about fuel cell stack. Fig. 8 shows a schematic of the inlet and outlet streams in a typical PEM fuel cell system. Hydrogen, air and cooling water are independent streams. Energy balance about the fuel cell stack was performed to calculate various energy terms associated with fuel cell operation:

$$q_{theo} = q_{elec} + q_{sens} + q_{latent} + q_{loss} \quad (13)$$

where q_{theo} is the theoretical energy produced by the fuel cell reaction, it is the total heat amount supplied to the stack; q_{sens} the sensible heat change calculated for each of the fuel cell streams (anode, cathode, and water coolant) which caused by the temperature and flowrate difference between the inlet and exit; q_{latent} is the total latent heat of the water vapourization (condensation) for anode and cathode streams; q_{elec} the electrical energy output, and q_{loss} the heat loss from the surface of the stack to the ambient. In steady case, by the first law of thermodynamics, total energy provided to the stack is equal to the sum of these four terms of energy, which either newly generated or with the amount changed. Comparing (13) with the model used in [33], the model developed in the present work included the two-phase effect (phase-change).

3.3.1 Energy equations:

Theoretical energy from the electrochemical reaction in PEM fuel cell was calculated through the product of reaction energy ΔH_{rxn} and molar flow rate of consumed hydrogen N_{H2cons} :

$$q_{theo} = N_{H2,cons} \Delta H_{rxn} \quad (14)$$

ΔH_{rxn} stands for the heat released by chemical reaction of hydrogen plus oxygen to form water, its values depend on the water product stage, if the water product is in liquid stage, $\Delta H_{rxn} = -286\text{kJ/mol}$, called high heating value; if the water product is in vapour stage, $\Delta H_{rxn} = -241\text{kJ/mol}$, called low heating value. The electrical power generated by the PEM fuel cell stack with n single cells was evaluated as:

$$q_{elec} = nV_{cell}i \quad (15)$$

The sensible heat change through anode stream was considered for all the possible species in anode (i.e., water vapour, liquid water, carbon dioxide from reformat) as follows:

$$\begin{aligned} q_{sens,a} = & N_{H_2,a,out} C_{p,H_2,g} (T_{a,out} - T_0) + N_{w,g,a,out} C_{p,H_2O,g} (T_{a,out} - T_0) + N_{co_2,a,out} C_{p,co_2,g} (T_{a,out} - T_0) \\ & + N_{w,l,a,out} C_{p,w,l,out} (T_{a,out} - T_0) - N_{w,l,a,in} C_{p,w,l,in} (T_{a,in} - T_0) - N_{w,g,a,in} C_{p,H_2O,g} (T_{a,in} - T_0) \\ & - N_{H_2,a,in} C_{p,H_2,g} (T_{a,in} - T_0) - N_{co_2,a,in} C_{p,co_2,g} (T_{a,in} - T_0) \end{aligned} \quad (16)$$

Here we account how much energy was brought into the stack and how much took away from the stack by anode stream.

The latent heat through the anode was included through tracking down the phase change (in the thesis, the water vapour and water liquid were assumed to be in equilibrium all the time, i.e., the condensation/evapouration process was assumed to be so fast that there is no finite condensation/evapouration rate; also the water transfer across the membrane was assumed in vapour form, see details for this assumption in [19]):

$$q_{latent,a} = (N_{w,g,a,out} - N_{w,g,a,in} + N_{trans}) H_{vaporization,a} \quad (17)$$

The sensible heat in cathode was considered in a similar way to that in anode except the species are different from those in anode. In cathode the species include oxygen, nitrogen, water vapour, water liquid, as shown in (13):

$$\begin{aligned} q_{sens,c} = & N_{O_2,c,out} C_{p,O_2,g} (T_{c,out} - T_0) + N_{w,g,c,out} C_{p,H_2O,g} (T_{c,out} - T_0) + N_{N_2,c,out} C_{p,N_2,g} (T_{c,out} - T_0) \\ & + N_{w,l,c,out} C_{p,w,l,out} (T_{c,out} - T_0) - N_{w,l,c,in} C_{p,w,l,in} (T_{c,in} - T_0) - N_{w,g,c,in} C_{p,H_2O,g} (T_{c,in} - T_0) \\ & - N_{O_2,c,in} C_{p,O_2,g} (T_{c,in} - T_0) - N_{N_2,c,in} C_{p,N_2,g} (T_{c,in} - T_0) \end{aligned} \quad (18)$$

The latent heat in cathode is somehow complicated due to the water generation, water phase change and transfer across the membrane. The basic rule here is to figure out the molar flow rate of the water vapour that is involved in phase change. Details are as follows:

For latent heat in cathode, if $N_{w,l,c,in} \geq (N_{w,g,c,out} - N_{trans} - N_{w,g,c,in})$, i.e., the amount of liquid water carried from the cathode inlet is big enough for phase change, then we have

$$q_{latent,c} = (N_{w,g,c,out} - N_{trans} - N_{w,g,c,in})H_{vaporization1,c1} \quad (19)$$

Otherwise, the liquid water carried from the inlet must be evaporated and some of product water must be evaporated too, so we have

$$q_{latent,c} = N_{w,l,c,in}H_{vaporization,c1} + (N_{w,g,c,out} - N_{trans} - N_{w,g,c,in} - N_{w,l,c,in})H_{vaporization,c2} \quad (20)$$

$$\text{where } H_{vaporization} = 45070 - 41.9T + 3.44 \times 10^{-3}T^2 + 2.54 \times 10^{-6}T^3 - 8.98 \times 10^{-10}T^4 \quad (21)$$

and subscripts c1 and c2 represent the different state (thus different temperature) for the evaporation of water that are from different origin, e.g., either from inlet stream or electrochemical product. Equation (21) is from [1].

The sensible heat in water coolant stream was calculated by use of the following formula:

$$q_{sens,w} = N_{w,in}C_{p,w,l}(T_{w,out} - T_0) - N_{w,in}C_{p,w,l}(T_{w,in} - T_0) \quad (22)$$

Then the sensible and latent heats were summed and the heat loss from the stack to the ambient was calculated based on (13):

$$q_{sens} = q_{sens,a} + q_{sens,c} + q_{sens,w} \quad (23)$$

$$q_{latent} = q_{latent,a} + q_{latent,c} \quad (24)$$

$$q_{loss} = q_{theo} - q_{elec} - q_{sens} - q_{latent} \quad (25)$$

3.3.2 Flow rates

The water vapour saturation pressure (atm.) was calculated based on the following equation [19]:

$$P_{w,g}^{sat} = 10^{-2.1794 + 0.02953 T - 9.1837 \times 10^{-5} T^2 + 1.4454 \times 10^{-7} T^3} \quad (26)$$

The molar flow rate for hydrogen in anode and air in cathode on dry condition at each inlet can be evaluated according to the operating current and excess coefficient [37] on each stream inlet:

$$N_{a,H_2,in,dry,0} = \frac{1}{2\beta_{H_2}} I \alpha_{H_2} n_e \quad (27)$$

$$N_{c,air,in,dry,0} = \frac{1}{4\beta_{O_2}} I \alpha_{O_2} n_e \quad (28)$$

where $n_e = 1.0365 \times 10^{-5} \text{ mol} / \text{A} \cdot \text{s}$ is the molar flow rate of electrons for generating 1 A electricity; α is excess coefficient i.e., the ratio of the actual amount supplied to the theoretical amount needed, and β is the molar fraction of oxygen in air stream at cathode inlet.

The equations of flow rates were proposed to account for the inlet water (liquid + vapour), as listed below:

The maximum water vapour carried from the anode inlet was evaluated as:

$$N_{w,g,a,in,max} = (N_{H_2,a,in} + N_{CO_2,a,in}) \frac{P_{w,g,a,in}^{sat}}{P_{a,in} - P_{w,g,a,in}^{sat}} \quad (29)$$

Then the amount of water vapour and water liquid at the anode inlet were calculated as below:

$$\text{If } N_{w,a,in} \geq N_{w,g,a,in,max} \text{ , then we have } \begin{cases} N_{w,g,a,in} = N_{w,g,a,in,max} \\ N_{w,l,a,in} = N_{w,a,in} - N_{w,g,a,in} \end{cases} \quad (30)$$

$$\text{If } N_{w,a,in} < N_{w,g,a,in,max} \text{ , then we have } \begin{cases} N_{w,g,a,in} = (N_{H_2,a,in} + N_{CO_2,a,in}) \frac{P_{w,g,a,in}^{sat} \phi_{a,in}}{P_{a,in} - P_{w,g,a,in}^{sat} \phi_{a,in}} \\ N_{w,l,a,in} = 0 \end{cases} \quad (31)$$

The maximum amount of water vapour at anode outlet was calculated as follows:

$$N_{w,g,a,out,max} = (N_{H_2,a,out} + N_{CO_2,a,out}) \frac{P_{w,g,a,out}^{sat}}{P_{a,out} - P_{w,g,a,out}^{sat}} \quad (32)$$

Then the amount of water vapour and water liquid in the anode outlet were evaluated as below:

$$\text{If } N_{w,a,in} - N_{trans} \geq N_{w,g,a,out,max} \text{ , then we have } \begin{cases} N_{w,g,a,out} = N_{w,g,a,out,max} \\ N_{w,l,a,out} = N_{w,a,in} - N_{trans} - N_{w,g,a,out} \end{cases} \quad (33)$$

$$\text{If } N_{w,a,in} - N_{trans} < N_{w,g,a,out,max} \text{ , then we have } \begin{cases} N_{w,g,a,out} = N_{w,a,in} - N_{trans} \\ N_{w,l,a,out} = 0 \end{cases} \quad (34)$$

For cathode inlet, the maximum water vapour carried from the cathode inlet was evaluated as:

$$N_{w,g,c,in,max} = (N_{O_2,c,in} + N_{N_2,c,in}) \frac{P_{w,g,c,in}^{sat}}{P_{c,in} - P_{w,g,c,in}^{sat}} \quad (35)$$

Then the amount of water vapour and water liquid in the cathode inlet were evaluated as below:

$$\text{If } N_{w,c,in} \geq N_{w,g,c,in,max}, \text{ then we have } \begin{cases} N_{w,g,c,in} = N_{w,g,c,in,max} \\ N_{w,l,c,in} = N_{w,c,in} - N_{w,g,c,in} \end{cases} \quad (36)$$

$$\text{If } N_{w,c,in} < N_{w,g,c,in,max}, \text{ then we have } \begin{cases} N_{w,g,c,in} = (N_{O_2,c,in} + N_{N_2,c,in}) \frac{P_{w,g,c,in}^{sat} \phi_{c,in}}{P_{c,in} - P_{w,g,c,in}^{sat} \phi_{c,in}} \\ N_{w,l,c,in} = 0 \end{cases} \quad (37)$$

In cathode stream, the water was produced and the product water was assumed to be liquid in the present study. It was evaluated as:

$$N_{w,l,prod} = N_{H_2,cons} = N_{H_2,a,in} - N_{H_2,a,out} \quad (38)$$

For cathode outlet, the maximum water vapour carried from the cathode outlet was evaluated as:

$$N_{w,g,c,out,max} = (N_{O_2,c,out} + N_{N_2,c,out}) \frac{P_{w,g,c,out}^{sat}}{P_{c,out} - P_{w,g,c,out}^{sat}} \quad (39)$$

Then the amount of water vapour and water liquid in the cathode outlet were evaluated as below:

$$\text{If } (N_{w,c,in} + N_{w,l,prod} + N_{trans}) \geq N_{w,g,c,out,max}, \text{ then we have } \begin{cases} N_{w,g,c,out} = N_{w,g,c,out,max} \\ N_{w,l,c,out} = N_{w,c,in} + N_{w,l,prod} + N_{trans} - N_{w,g,c,out} \end{cases} \quad (40)$$

$$\text{If } (N_{w,c,in} + N_{w,l,prod} + N_{trans}) < N_{w,g,c,out,max}, \text{ then we have}$$

$$\begin{cases} N_{w,g,c,out} = N_{w,c,in} + N_{w,l,prod} + N_{trans} \\ N_{w,l,c,out} = 0 \end{cases} \quad (41)$$

The average heat transfer coefficient for the stack may be estimated using the average heat loss from the surface of the fuel cell stack. Similarly, the increase in sensible and latent heat terms could also be linked to heat transfer coefficients, h_j , from the stack to the fluid j , where $j =$ anode, cathode, or water stream. Once heat transfer coefficients h , heat exchange area and sensible, latent heat terms are known, the temperature of stack and outlet flows could be estimated by using the following equations:

$$T_{stack} = \frac{q_{loss}}{(hA)_{stack}} + T_{room} \quad (42)$$

$$T_{a,out} = 2\left[T_{stack} - \frac{q_{sen,a} + q_{latent,a} + q_{mass,a}}{(hA)_a}\right] - T_{a,in} \quad (43)$$

$$T_{c,out} = 2\left[T_{stack} - \frac{q_{sen,c} + q_{latent,c} - q_{mass,c}}{(hA)_c}\right] - T_{c,in} \quad (44)$$

$$T_{w,out} = 2\left[T_{stack} - \frac{q_{sen,w}}{(hA)_w}\right] - T_{w,in} \quad (45)$$

where the energy change due to mass transfer and mass consumption (including the sensible energy carried by the water transfer across the membrane, the sensible energy carried by hydrogen/oxygen consumed) was evaluated as follows.

$$q_{mass,a} = N_{trans} C_{p,H_2O,g} (T_{stack} - T_0) + N_{H_2,con} C_{p,H_2,g} (T_{stack} - T_0) \quad (46)$$

$$\begin{aligned} q_{mass,c} = & N_{trans} C_{p,H_2O,g} (T_{stack} - T_0) + N_{H_2,con} C_{p,H_2O,l} (T_{stack} - T_0) \\ & - N_{O_2,con} C_{p,O_2} (T_{stack} - T_0) \end{aligned} \quad (47)$$

3.4 Transient model

In the transient state, an additional accumulation term should be considered, therefore:

$$m_{stack} C_{p,stack} \frac{dT_{stack}}{dt} = q_{theo} - q_{elec} - q_{sens} - q_{latent} - q_{loss} \quad (48)$$

where m is the total mass of the fuel cell stack, C is the average specific heat of the stack, and dT_{stack}/dt is the temperature change with respect to time. From Equation (48), we have

$$\frac{dT_{stack}}{dt} = \frac{q_{theo} - q_{elec} - q_{sens} - q_{latent} - q_{loss}}{m_{stack} C_{p,stack}} \quad (49)$$

In the calculations presented, an average value of 35kJ/K was used for $m_{stack} C_{p,stack}$ of Ballard Mark V stack. Knowing all the terms on the right side of the Equation (49), it could be used as a basis of a finite-difference calculation using:

$$T_{stack}^{new} = T_{stack}^{old} + \frac{dT_{stack}}{dt} \Delta t \quad (50)$$

once we get the stack temperature's derivative with time in Equation (49), given one time step value, use stack temperature value at the beginning of one time step, we can calculate the temperature at the end of time step using (50).

3.5 Pressure drop

Pressure drop along the channels could be calculated by using average gas velocity, which is the mean value of inlet and outlet velocity of each stream. Ignoring the volume of liquid water, the local velocity V (m/s) was determined by gas molar flow rate (mol/s), local pressure, temperature, cross-section area of channel A_c , and number of channels (N_{ch}).

$$V = \frac{N \times 22.4 \times 10^{-3} \frac{p_0}{p} \frac{T}{T_0}}{A_c N_{ch}} \quad (51)$$

where the gas molar flow rate could be determined for each stream as follows:

$$\text{at anode inlet,} \quad N = (N_{H_2,a,in} + N_{CO_2,a,in}) \left(1 + \frac{p_{w,g,a,in}^{sat} RH_{a,in}}{p_{a,in} - p_{w,g,a,in}^{sat} RH_{a,in}} \right) \quad (52)$$

$$\text{at anode outlet,} \quad N = (N_{H_2,a,out} + N_{CO_2,a,out}) \left(1 + \frac{p_{w,g,a,out}^{sat} RH_{a,out}}{p_{a,out} - p_{w,g,a,out}^{sat} RH_{a,out}} \right) \quad (53)$$

$$\text{at cathode inlet,} \quad N = (N_{O_2,c,in} + N_{N_2,c,in}) \left(1 + \frac{p_{w,g,c,in}^{sat} RH_{c,in}}{p_{c,in} - p_{w,g,c,in}^{sat} RH_{c,in}} \right) \quad (54)$$

$$\text{at cathode outlet,} \quad N = (N_{O_2,c,out} + N_{N_2,c,out}) \left(1 + \frac{p_{w,g,c,out}^{sat} RH_{c,out}}{p_{c,out} - p_{w,g,c,out}^{sat} RH_{c,out}} \right) \quad (55)$$

When $RH = 1$, the largest molar flow rate for each stream is obtained. Once temperature and flow rate are known, the pressure drop along the channels could be obtained by using (Darcy-Weisbach equation [38]):

$$\Delta p_a = f_a \times \frac{L_a}{D_a} \frac{\rho_a V_{a,m}^2}{2} \quad (56)$$

$$\Delta p_c = f_c \times \frac{L_c}{D_c} \frac{\rho_c V_{c,m}^2}{2} \quad (57)$$

where D is the hydraulic diameter. Equation (56) and (57) are used to calculate single phase pressure drop in the anode channel and the cathode channel, f_a and f_c are the friction factor which are decided by the channel shape and flow Reynolds number. Inside the anode channel, because no water is produced, the flow regime is in laminar flow, (56) is good enough when we ignore the volume of the inlet water liquid. For the cathode channel, product water is in liquid stage, the flow is defined as two-phase (vapour and liquid water, two component (air and water), we will use the modified formula based on (57). See chapter 4. Two-Phase Flow Study in Cathode Channel for details.

3.6 Water transfer across membrane

Water transfer across membrane is the sum of following three terms [19, 39]:

1. Electro-osmotic drag flux, which is caused by hydrogen ion drag. When hydrogen ions go through membrane, each of them will carry some water molecule with them from anode to cathode.
2. Diffusion flux, which is caused by water concentration gradient between anode and cathode. The direction of this flux depends on which side has higher water vapour concentration.

3. Convection flux, which caused by water vapour pressure gradient between anode and cathode. The direction of this flux depends on which side has higher water vapour partial pressure.

$$\text{Therefore, } N_{trans} = N_{drag} + N_{diff} + N_{conv} \quad (58)$$

The electro-osmotic drag flux could be calculated by [19, 39]:

$$N_{drag} = n_d \frac{I(x)}{F} \quad (59)$$

$$n_d = \frac{2.5}{22} \lambda \quad (60)$$

$$\begin{aligned} \lambda &= 0.043 + 17.81a - 39.85a^2 + 36.0a^3 \quad \text{at}(a < 1) \\ &= 14.0 + 1.4(a - 1) \quad \text{at}(3 \geq a \geq 1) \\ &= 16.8 \quad \text{at}(a \geq 3) \end{aligned} \quad (61)$$

$$a = \frac{P_{vapor}}{P_{sat}} \quad (62)$$

where n_d is called electro-osmotic drag coefficient; I is the current density; a is water vapour activity (ratio of the water vapour pressure and the saturation pressure); λ is the water content of membrane that is related with water vapour activity.

The diffusion drag flux is decided by diffusion coefficient D_m , water concentration c and the membrane charge concentration c_f which is fixed for one type of membrane [19, 39].

$$\begin{aligned} D_m &= 10^{-10} \exp[2416(\frac{1}{303}) - (\frac{1}{T})] (2.563 - 0.33\lambda + 0.0264\lambda^2 - 0.000671\lambda^3) \quad \text{at}(\lambda > 4) \\ &= 10^{-10} \exp[2416(\frac{1}{303}) - (\frac{1}{T})] (-1.25\lambda + 6.65) \quad \text{at}(4 \geq \lambda \geq 3) \\ &= 10^{-10} \exp[2416(\frac{1}{303}) - (\frac{1}{T})] (2.05\lambda - 3.25) \quad \text{at}(3 > \lambda \geq 2) \end{aligned} \quad (63)$$

$$c = \lambda c_f \quad (64)$$

$$N_{diff,y} = -D_m \frac{dc}{dy} = -D_m c_f \frac{d\lambda}{dy} \quad (65)$$

Convection flux was calculated as follows:

$$N_{conv,y} = -\frac{k_p}{\mu} c \frac{dp_v}{dy} = -\frac{k_p}{\mu} \lambda c_f \frac{dp_v}{dy} \quad (66)$$

where k_p , μ , dp_v and c are the hydraulic permeability of water in membrane, water viscosity, partial pressure difference between the anode and cathode, and concentration of water in membrane.

Water management is very important for stack operation because membrane with proper amount of water will increase membrane conductivity. In our electro-chemical model we have mentioned that high membrane conductivity will produce higher voltage output by reducing ohmic overpotential, now we use the formula here [19]:

$$\sigma_m = \exp\left[1268\left(\frac{1}{303} - \frac{1}{T}\right)\right] \times (0.5139\lambda - 0.326), \text{ for } \lambda > 1 \quad (67)$$

From Equation (67) we see that the membrane conductivity σ_m is decided by the water content of membrane λ , and λ depends on the water activity of both sides, the membrane conductivity will be reduced if either side has a low water vapour amount. In most cases, water transfer is from the anode side to the cathode side because the Electro-osmotic drag flux is dominant amount, it will cause dry anode stream at anode side. How to keep the anode stream moist is the key point of water management. Letting in some liquid water from the reservoir of evaporation source is an effective method, but on the other hand, if the stream contains too much water liquid, it will block the porous of

membrane, making it difficult for ions go through. From previous operating experiences, when the stack temperature is over 60°C external humidify device must be employed to keep stream moist. This will increase the system cost and it is impossible for some application with strict space limitation, therefore, in some miniature fuel cell system lower efficiency without extra humidification is the only choice.

3.7 Calculation of air compressor

Whatever type of compressor is selected, the efficiency related calculations are same. Below we will discuss the compressor consumed power calculation. The equations in this section are all from [1]. Suppose in adiabatic process, the suction/output air pressure is p_1 and p_2 then the temperature will increase from T_1 to T_2 , where:

$$\frac{T_2}{T_1} = \left(\frac{p_2}{p_1} \right)^{\frac{\gamma-1}{\gamma}} \quad (68)$$

γ is the ratio of the specific heat capacities of the gas c_p/c_v . There are three assumptions to be used to simplify our calculation:

1. The heat generated by mechanism (impossible for all mechanical work contribute to compression, some will change to heat energy) is negligible.
2. The change of kinetic energy between inlet gas and outlet gas are negligible.
3. During the compression, gas specific heat at constant pressure c_p is constant.

Under above assumptions, the mechanical work done will only change the gas enthalpy, the below formula will hold:

$$\dot{W} = c_p (T_2 - T_1) \dot{m}_{gas} \quad (69)$$

\dot{m}_{gas} is the mass rate of the compressed gas. In fact, above formula is in isentropic process, in the real work, the exit temperature will be higher than the isentropic one, so

$$\dot{W}' = c_p (T_2' - T_1) \dot{m}_{gas} \quad (70)$$

hold for the real work, \dot{W}' and T_2' are the real work of compression and the real exit temperature. The ratio between isentropic work and the real work is isentropic efficiency,

$$\eta_{cp} = \frac{\text{isentropic work}}{\text{real work}} = \frac{c_p (T_2 - T_1) \dot{m}_{gas}}{c_p (T_2' - T_1) \dot{m}_{gas}} = \frac{T_2 - T_1}{T_2' - T_1} \quad (71)$$

Combine (69) into (71), we have

$$\eta_{cp} = \frac{T_1}{T_2' - T_1} \left[\left(\frac{p_2}{p_1} \right)^{\frac{\gamma-1}{\gamma}} - 1 \right] \quad (72)$$

and the temperature difference will be:

$$\Delta T = T_2' - T_1 = \frac{T_1}{\eta_{cp}} \left[\left(\frac{p_2}{p_1} \right)^{\frac{\gamma-1}{\gamma}} - 1 \right] \quad (73)$$

Combine (69) and (73) we have

$$Power = \dot{W}' = c_p \frac{T_1}{\eta_{cp}} \left[\left(\frac{P_2}{P_1} \right)^{\frac{\gamma-1}{\gamma}} - 1 \right] \dot{m}_g \quad (74)$$

Equation (74) is for the calculation of the power needed to drive a compressor. Consideration should be given to the power loss during the transfer from electrical motor to compressor, e.g. mechanical efficiency η_m , which value is very high for centrifugal and axial type, over 98%.

Once we know the gas physical properties data, inlet temperature, mass flow rate, compressor efficiency and suction/output pressure, we can calculate the dynamic power consumed by the compressor, and count this part into the stack system efficiency calculation to optimize stack operation.

3.8 Calculation of cooling pump

The cooling system is a closed loop. The power provided by the water pump will be used to overcome the friction loss and keeps fluid running at one certain velocity inside, pump in system is shown at Fig. 9 and all equations in this section are from [38].

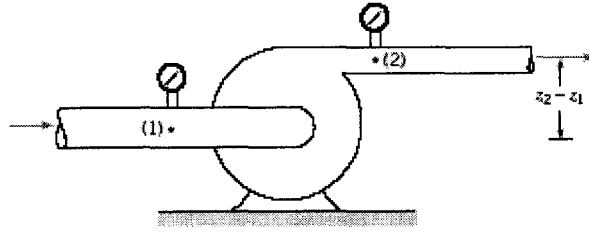


Fig. 9. Pump for coolant [53]

The formula for the pumping power will hold as:

$$\left[\frac{p_2}{\rho_2} - \frac{p_1}{\rho_1} \right] + \left[\frac{u_2^2}{2} - \frac{u_1^2}{2} \right] + g(z_2 - z_1) = h_{wp} g \quad (75)$$

The subscript 2 and 1 stand for pump inlet and outlet respectively. p , ρ and u are the pressure, density and velocity (respectively) of the water flow; g and z for gravity and head; W_{wp} is the pumping power received by fluid; h_{wp} is the head rise actually gained by fluid through pump. If we ignore the differences of density and the head between the inlet and outlet, and also assume inlet water velocity is zero (water intake from water tank), the simplified equation for the pumping power is:

$$h_{wp} = \frac{p_2 - p_1}{\rho g} + \frac{u_2^2}{2g} \quad (76)$$

The calculation of fraction loss along the channel can be found in Equation (57), (86) in the pressure drop part in this thesis. The pumping power received by fluid can be expressed as:

$$\dot{W}_{wp} = h_{wp} \rho g \dot{m} \quad (77)$$

Once we get the pumping power needed for the fluid and know the characteristic curves for a selected pump, we can find out the real power consumed by the cooling system.

3.9. Calculation case and pump characteristic curves

The consumed power by compressor and pump in fuel cell system will be used to calculate the net power output and system efficiency. For calculation purpose, of course we can not go over all the application cases. In this thesis, we just provide one general calculation method of system efficiency by considering pump and compressor. In real system application, different type of pump and compressor might be selected, but the basic calculation methods are same. Once we select one type of water pump and compressor, we will get the efficiency curves at different mass flow rates. Fig. 10 is a generic pump characteristic curve plotting. BHP curves in Fig. 10 stands for pump input or brake horsepower, is the actual horsepower delivered to the pump shaft. The pump curve is the pumping head provided by the pump, it will decrease with the flow rate goes up. Efficiency curve stands for the pump efficiency under different flow rates, at one fixed flow rate, the pumping power of the pump equals its BHP value times the efficiency. Once we know the fuel cell operating flow rate, we select the pump whose operating point located at that flow rate, because only at operating point's flow rate, the pump will have highest efficiency. The operating flow rate higher than the value at the operating point or lower than that value will consume more electrical power. In our simulation calculation, we use pump efficiency value = 70% at the operating point, this value should be changed once the specific pump curve is employed.

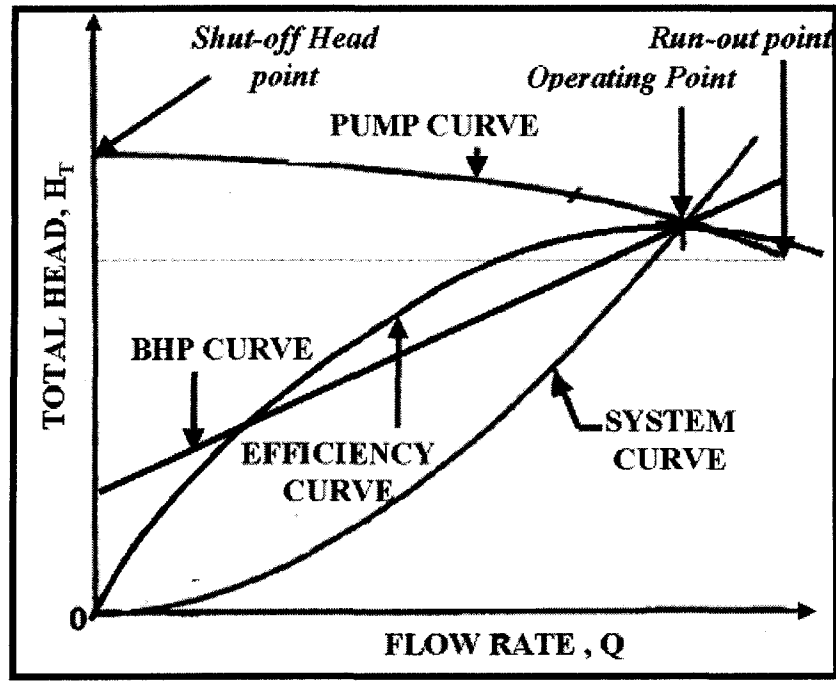


Fig. 10. Pump characteristic curve under different flow rates and pressures [54]

The compressor will take some time to reach full running speed from a rest state. A stopped compressor would prevent a fuel cell stack run into its steady condition by being air-starved for a short period of time. In some applications, such as automotive industrial, there is a requirement for the stack of start up and accelerating as fast as it could. One possible solution is to maintain an elevated minimum flow rate for the compressor even at low power output, the system efficiency will suffer.

4. TWO-PHASE FLOW STUDY IN CATHODE CHANNEL

4.1 General introduction

Water plays an important role in PEM fuel cell operation. Well water management inside the fuel cell channel will increase stack power output, otherwise, the phenomenon of lower current density or lower cell voltage will be observed, resulting in either water flooding or dry membrane. One more important issue is water (both liquid and vapour) will impact the heat transfer between the stack channels and the stream flows. Considerations must be given to the affection of water when we do the thermal calculation. On the anode side, water will be injected into the channel with the reactant gas, no water product in the anode channel, the amount of water will depend on the inlet condition only (we use relative water content ϕ to calculate the amount of both water vapour and water liquid). Because water transfer across the membrane is from the anode to the cathode side, this transfer will cause unsaturated vapour in the anode channel, so except near the entrance at $\phi > 1$, no liquid water exist inside the anode channel. We can treat the anode stream as one phase flow when we do heat transfer and pressure drop calculation as we have discussed in section 3.3 and 3.5. It is quite a different story with the anode. The total water amount on the cathode side will be the sum of the inlet water, water dragged from the anode side and the water product. These three parts of water will make a rich reservoir for vaporization when stream temperature increased, the left amount of water will still be in liquid stage during the process of heat transfer, the participation of liquid water make the heat transfer on the cathode side more complicated

than the anode side. We can not just treat it as a one-phase flow in our calculation, and this topic will be discussed more in detail later.

In PEM fuel cell applications, regarding the temperature range of stack solid and streams, the cathode flow pattern should be defined as two-phase (water vapour and liquid), and two-component (water and air) flow; The heat transfer is in non-boiling field. Unlike conventional flow of this type, we are facing two challenges here. First the hydraulic diameter of PEM fuel cell channel is about 1-2mm, it belongs to the mini-channel flow from the definition of fluid mechanics, some analytical methods and empirical formulas on conventional size don't work well here; Second the large flow volume ratio between liquid water and gas (over 4%) is beyond the most application cases, a few experimental data reported on this case. When we start cathode channel heat transfer and pressure drop study, we focus on the literature review of two-phase, two-component flow in mini-channel flow, calculate original flow data of different stack operation conditions to define the flow regime, at last to find out how to calculate heat transfer flux and the pressure drop with analogy.

In this context, two phase flow refers to the fact that the flow along the channel water may in liquid and/or vapour stages and the liquid evaporation and vapour condensation will happen during the phase change inside channel. The related latent heat has already been considered in the general energy balance equation (section 3.3), so we don't need to mention it again. Water liquid and air flow are the two components of the cathode channel flow. The air water mixed flow will present different flow patterns at different component flow ratio. These are: stratified, wavy, slug and annular. Also each different

Table 1. Cathode channel flow data

Working current (A)	O2 flow rate (mol/s)	Liquid product rate (mm ³ /s)	Air Re number	u_g^s (mm/s)	u_l^s (max) (mm/s)
20	0.004	2.06	831	2844	1.37
40	0.008	4.12	1662	5688	2.74
60	0.012	6.17	2494	8533	4.11
80	0.016	8.25	3325	11377	5.48
100	0.020	10.31	4156	14222	6.85
120	0.024	12.33	4988	17066	8.22
140	0.028	14.40	5819	19911	9.60
160	0.032	16.49	6650	22755	10.97
180	0.036	18.56	7482	25600	12.34
200	0.040	20.62	8313	28444	13.71

From Table 1, we can see that compare to gas superficial velocity the liquid one is quite small and the ratio is fixed, this is because during the reaction, the ratio between air consumption rate and the liquid water product rate keeps the same all the time in (1). From the Reynolds number we know the flow is laminar for all different stack operating conditions. These data will be used to judge the flow regime. Yemada Taitel and A.E. Dukler [40] used four dimensionless Martinelli parameters: X, F, T, K to predict horizontal flow regime, $C_g = C_l = 16$, $n = m = 1$ for laminar flow, so in our cases, the calculation formula are as follows:

$$X = \left[\frac{(dp/dx)_g^s}{(dp/dx)_l^s} \right]^{1/2} = \left[\frac{\frac{4C_l (u_l^s D)^{-n} \rho_l (u_l^s)^2}{D v_l 2}}{\frac{4C_g (u_g^s D)^{-m} \rho_g (u_g^s)^2}{D v_g 2}} \right]^{1/2} = \left[\frac{\rho_l v_l u_l^s}{\rho_g v_g u_g^s} \right]^{1/2} \quad (78)$$

$$F = \sqrt{\frac{\rho_g}{(\rho_l - \rho_g)}} \frac{u_g^s}{\sqrt{Dg}} \quad (79)$$

$$T = \left[\frac{(dp/dx)_l^s}{(\rho_l - \rho_g)g} \right]^{1/2} \quad (80)$$

$$K = \left[\frac{\rho_g (u_g^s)^2 u_l^s}{(\rho_l - \rho_g)g v_l} \right]^{1/2} \quad (81)$$

The corresponding values of these four parameters under different operating currents are listed in Table 2. Once we have these parameter values, we can find out in which flow pattern the flow is by using Fig. 11, the reported flow regime map in [40]. Using MATLAB, we retrieve the formulas of the curve A and C which can be used to judge the flow regime in our computation programming. For curve A we have:

$$F = 0.3435X^{-0.306} \quad (82)$$

For curve C we have

$$K = 0.00291 \exp(0.1172X) + 4.88 \exp(-0.04485X) \quad (83)$$

Table 2: Dimensionless parameters for flow regime

Working current (A)	X	T	F	K
20	0.054	0.047	1.93	1.59
40	0.054	0.067	3.86	4.52
60	0.054	0.082	5.80	8.30
80	0.054	0.094	7.73	12.78
100	0.054	0.106	9.67	17.86
120	0.054	0.116	11.60	23.48
140	0.054	0.125	13.54	29.59
160	0.054	0.134	15.47	36.16
180	0.054	0.142	17.41	43.14
200	0.054	0.150	19.34	50.53

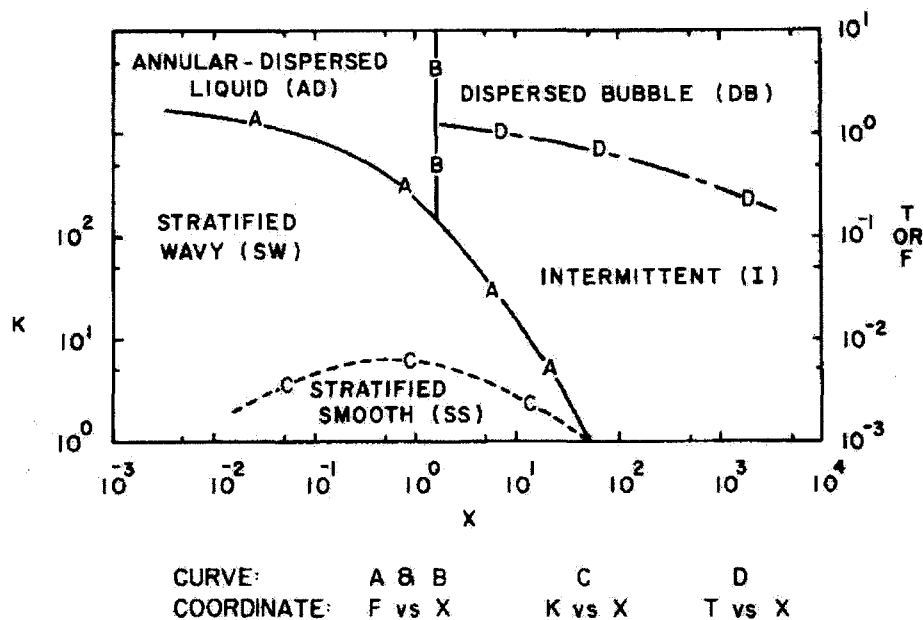


Fig. 11. Flow regime map from [40]

The value of F in our higher working current simulation is up to 19.34 which beyond the range of F in [40]. Higher F value stands for higher gas velocity, once run into annular dispersed flow region, continue increase the gas velocity will not change the flow type. So in our higher F value simulation case, the flow will still remain in annular type.

Compare the flow regime map [40] and our dimensionless data. The flow pattern inside the cathode channel is in Annular-Dispersed Liquid flow (curve A, use F vs X), also our data fall into the stratified smooth and wavy region (curve C, use K vs X). This means that there are two flow regimes inside the cathode channel, during the stack operations, cathode side flow regime will switch between annular-dispersed flow and stratified wavy flow.

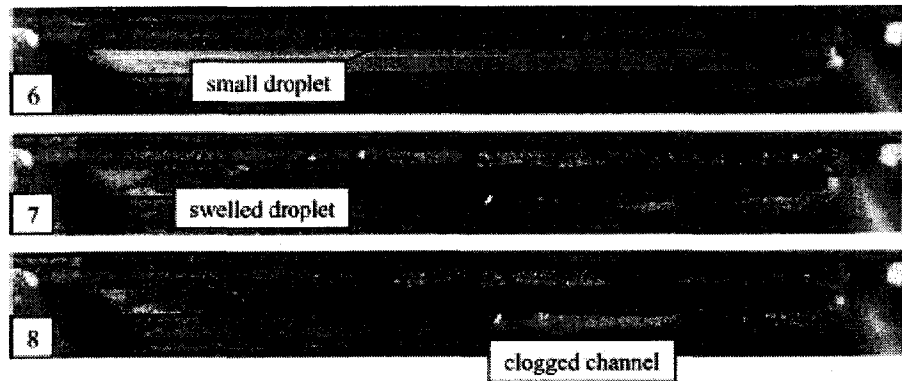


Fig. 12. Flow regime inside cathode channel [41]

Use the testing visualization picture from K. Tuber et al [41] we can explain why there have two flow regimes inside the cathode channel. Fig.12 shows the cathode channel operation with a hydrophobic diffusion layer, the channel parameters are Depth = 1mm; Height = 1.5mm; Length = 50 mm; V=0.5volt; A=0.35mA/cm². Above testing show that after 5 minutes operation, small droplets appear on the inner surface, then driven by the air flow, the droplet creeps along the surface. This stratified smooth flow regime will continue and turn into wavy regime during the water accumulation on the surface (about 30 min after start), then at some location, droplets keep growing to occupy most of the across section of the channel, the local air with higher velocity will blow the droplet away into many small pieces, the flow is in annular-dispersed regime. After this period, the flow go back to stratified again, so during the stack operation, the cathode channel water flow regime will keep this unsteady state between stratified and annular dispersed. The unsteady flow regime make it is difficult to do the heat transfer coefficient study.

To find the heat transfer data correctly, we introduce another flow regime judgment method provided by G. hetsronia *et al.* [42], they published the results after conducting

bench of experiments on a mini tube, and one result is shown in Fig. 13, the tube diameter $d = 1\text{mm}$, which is at the same order as our cathode channel. Their testing cases were under different superficial velocities of liquid and vapour, in Fig. 13 the range is 24-42m/s for gas velocity; liquid velocity is 0.016m/s, which is similar with our simulation cases at high operating current. Our gas superficial velocity is in the range of 3-28 m/s while the maximum liquid superficial velocity range in from 0.001m/s to 0.01m/s.

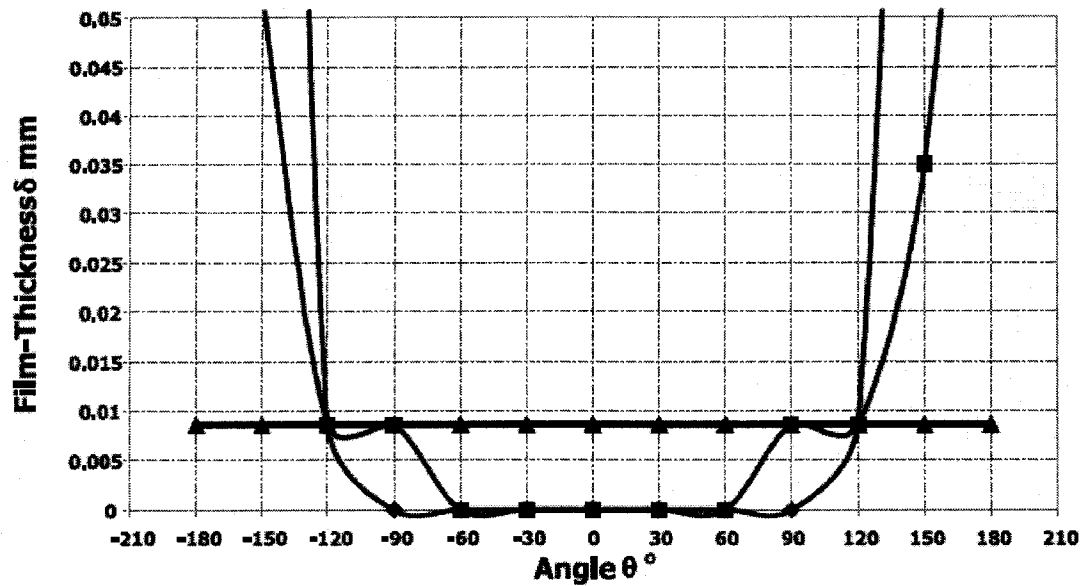


Fig. 13. Film-thickness distribution around circumference of the pipe near the upper point at $V_l^s = 0.016\text{m/s}$. V_g^s : (◆) 24m/s, (■) 36m/s, (▲) 42m/s in [42]

Fig. 13 shows three testing curves of water film thickness around the tube inside surface, while the air superficial velocity is 24m/s, 36m/s and 42m/s, the liquid velocity keep same at 0.016m/s. At low air velocity 24m/s and 36m/s, we can observe the thickness variation of water film on tube radial direction. At the upper region of the tube inside (near angle = 0°) the thickness is zero, it mean these is a dry out zone there. The thickness increased until reach its maximum near the tube bottom (angle = $\pm 180^\circ$). We

call this as opened annular water film. The film thickness is well-distributed at air velocity of 36m/s than 24m/s. At air velocity reaches 42m/s, the top dry out disappeared, we see the water film thickness is totally even on radial direction, we call this closed annular water film. The conclusion here is when liquid flow rate is quite low than air flow rate, the flow regime is annular and the higher air velocity, the more even water film thickness on tube radial direction.

Above testing physical condition is similar with our high current stack operating cases, for our low current operating cases, the absolute value of air velocity is not high as the testing one in [42], we need to discuss this situation here. When air flow rates is not high, at some place especially on inner surface upper region, the liquid layer puffs up and occupies a much larger area fraction of the pipe, then entrained into the gas in terms of some small droplets of liquid, with the moving along the channel, air may be threw droplets back to the liquid layer. Because there is a continuing production of liquid water on the inner surface and water liquid is removed away from the surface at the same time, in generally the liquid amount adhere on the surface keep same. From the radial view inside cathode channel, flow appears to consist of two distinct phases: an upper region consisting primarily of droplets/dry out and a lower region in the liquid film. For one fixed liquid superficial velocity, the higher are flow rate, the more even or less variation of the film thickness in radial. The experimental results on different tube diameters shows that when the air superficial velocity is high enough, the film forms a closed annular, and the thickness is same around the tube, no droplets and dry out near upper region. Comparing our air superficial velocity and the ratio, we can conclude that the film thickness is even (closed annular) for the cathode channel at higher current operation and

an upper dry out flow (opened annular) at lower current operation. Also from the results in [42], we know the film thickness is in the range of 0.01 mm, so we can ignore the cross-sectional area shrunk by film thickness when we calculate velocity parameters.

4.3 Heat transfer calculation/correlation

Most of two-phase flow heat transfer analyses are based on experiments. Equation (84) is the two-phase flow heat transfer coefficient from G. Hetsronia *et al.* [42], they use the heat transfer coefficient of single air phase flow h_g and correlate by liquid Froude number Fr_l and the flow superficial velocity ratio of air and liquid, the formula is:

$$\left(\frac{h}{h_g}\right) = 1 + 4.8 (Fr_l u_g^s / u_l^s)^{0.57} \quad (84)$$

$$Fr_l = u_{ls}^2 / gD \quad (85)$$

In Table 3, we list the heat transfer coefficients in our operating cases, including single air phase h_g and the two-phase h calculated by (84).

Table 3. Heat transfer coefficients chart

Working current (A)	h_g (W/m^2K)	h (W/m^2K)	h/h_g	4.4 Pre sur e dro p calc
20	99.27	185.46	1.86	
40	99.27	289.22	2.91	
60	99.27	400.85	4.03	
80	99.27	517.90	5.21	
100	99.27	639.16	6.43	
120	99.27	763.89	7.69	
140	99.27	891.58	8.98	
160	99.27	1021.85	10.29	
180	99.27	1154.43	11.62	
200	99.27	1289.10	12.98	

ulation/correlation

Pressure drop is another important characteristic in the design of fuel cell stack, correct calculation of the pressure drop will help designer to select compressor and pump. For optimum performance, it is necessary to minimize the pressure drop in the flow of gases through the stack as pumping power also reduces the overall efficiency of the system. Same challenges as we met in heat transfer, most pressure drop studies on the two-phase flow focus on the case with hydraulic diameter is larger than 10 mm. However, in fuel cell application, mini-channel with the smaller tube diameter will increase pressure drop due to the increase of the wall friction. When we review pressure drop paper on two-phase flow, we find that most of research jobs are from Lockhart–Martinelli Correction, which formula is based on the single phase flow frictional pressure gradient $(dp/dx)_l$, corrected by the two-phase frictional multiplier ϕ_l , $C = 5$ is used here and these values are defined as:

$$(dp/dx)_{TP} = \phi_l^2 (dp/dx)_l \quad (86)$$

$$\phi_l^2 = 1 + \frac{C}{X} + \frac{1}{X^2} \quad (87)$$

$$X = [(dp/dx)_l / (dp/dx)_g]^{1/2} \quad (88)$$

In most engineering applications, traditional Lockhart–Martinelli correlation is adequate to predict the two-phase pressure drop. But due to the fact that based on single liquid phase and set up for the conventional channel size, it could not represent the experimental results at the condition of low liquid superficial velocity and the flow in mini-channels, these are reported by Fujita *et al.* [43], Ide and Matsumura [44], Lowry and Kawaji [45] after examined the different flow patterns of air water flow in series of

small diameters. Here we introduce one new correlation to compare with traditional Lockhart–Martinelli correlation formula. One is from Mishima and Hibiki [46], the formula of correlation parameter is:

$$C = 21\{1 - \exp(-0.319D_h)\} \quad (89)$$

5. SOLUTION METHODOLOGY

5.1 Algorithm and the Interaction among Models

From previous introduction we know that behind our model there are bench of non-linear equations which include the unknown variables such as cell voltage, voltage loss, temperatures of both solid and streams, membrane conductivity and water transfer amount. These key variables are determined dynamically by cell working current, and the physical properties of each stream: flow rates, pressure, viscosity, Reynolds number and stream humidity rate.

Generally, the solving method of non-linear equations can be categorized into two catalogues: direct methods and iterative methods.

Direct method is quite straightforward, the relations between the variables are predefined, the unknown variables are formulated in term of known variables, once the input values are known, the values of corresponding unknowns will be calculated by these predefined formulas. Problems of direct method come from two sides, first for non-linear equations sometimes it is difficult or impossible to derive those predefined equations for unknown variables, and these expressions must be manipulated it manually. Second, in finite different method computation, large vectors and parallel architectures are involved duo to huge amount of the control volume in calculation domain. Before final result comes out, the computer had to keep these values in each control volume. It needs a large computer memory. Compare to direct method, iterative methods are relatively easy for computation no matter how large number of calculation domain is. At the end of each iteration, only output parameter values are kept and passed as the inlet

data by computer to the next round calculation until the result is satisfied. Computer will repeat same computation procedure so it will use less computer memory and easy to program than the direct methods. The tradeoff of iterative method calculation is that it will take longer time to repeat the same calculations in each recursion. For the reason of easy to compute, we use Gauss-Jacobi iteration calculation in our simulation. Use guessed values for all the unknown variables at the very beginning, these guessed values will be brought into equations to calculate the new one, iterative methods attempt to find the real solution by repeatedly solving the equations using approximations to the them. Iterations continue until the result is within a predetermined acceptable bound on the error.

For a better understanding of solution procedure, we use the Fig. 14 below to interpret the relation among those main variables in different model. From Fig. 14 we see that the main parameters of electro-chemical model is stack operating current, voltage output and membrane conductivity, these values could be calculated once Electro-chemical model obtain enough information on reaction temperature, fuel/air pressure on catalyst layer and humidification rate in channels from thermal model; also total water sources in channels water transfer amount across the membrane from water management model. As a return, after the operating current has been defined, electro-chemical model will provide energy balance information to thermal model, which include how much the energy released by chemical reaction is and how much heat is available for heat transfer inside stack, so the thermal arrangement (cooling degree) could be decided; The thermal model is based on the theory of fluid mechanics and heat transfer, such as the calculation of flow Reynolds number and channel pressure drop. During the temperature change of

solid and flow, the amount water evaporation and condensation are also calculated in thermal model and provide this information to water management model for the computation of the amount of water transfer across membrane. The water management model will feed back the total water available inside each channel to the thermal model for the humidification rate and liquid water amount calculation; The water management model will be informed with the stack current drag flux by electro-chemical model, then use this value to calculate water content of membrane which is deterministic to the values of membrane conductivity and resistance.

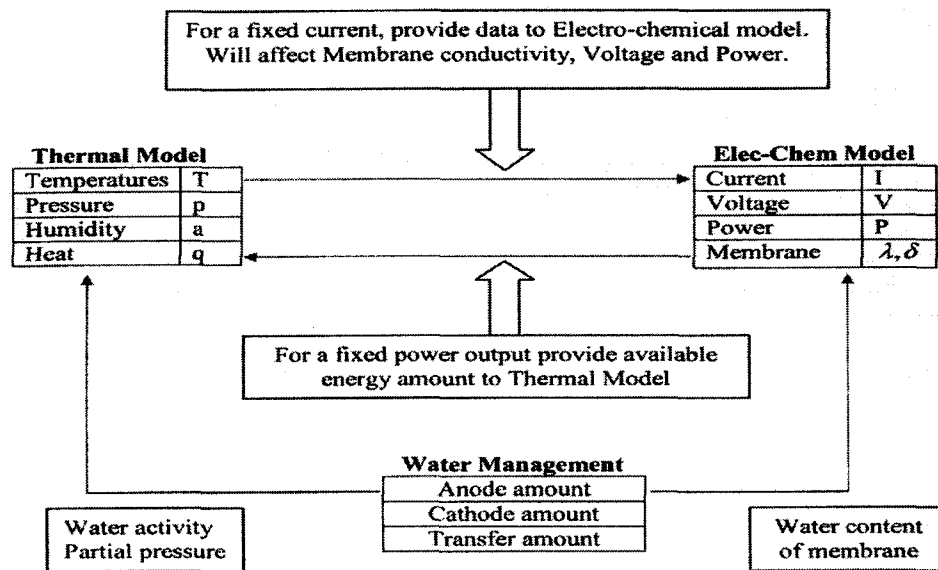


Fig. 14. Interaction between the parameters of different models

From above words we know that the main parameters among these three models are closely related, if one parameter gets a change, all corresponding data will change simultaneously. When stack runs into its steady state, all parameters keep the same unless the operating condition is changed. Once undergo a load perturbation, it will take some

time for the stack to reach a new steady state and parameters will change within this time period. We have different calculation methods for steady and unsteady cases.

5.2 Steady State Models

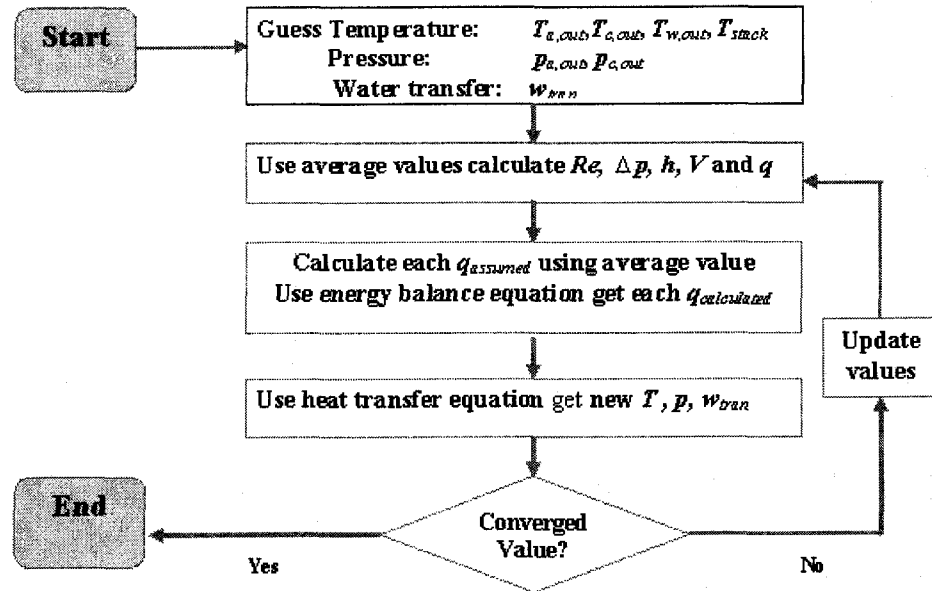


Fig. 15. Steady Case calculation methodology

Fig. 15 shows the steady state calculation methodology.

Step 1: Start with a guess or estimate for the values of temperature T_{stack} , $T_{w,out}$, $T_{a,out}$, $T_{c,out}$, pressure $p_{a,out}$, $p_{c,out}$ and the amount of water transfer across the membrane w_{tran} .

Step 2: From these guessed values, calculate thermal physical data first in thermal model, then pass these to electro-chemical model to get tentative values of V_{cell} and at last back to thermal model again to get related tentative energy terms.

Step 3: Use those tentative energy values and energy balance equation to get the new calculated values of related energy terms.

Step 4: Use those new calculated energy values and heat transfer coefficients to get new values of T and p .

Step 5: With these p , T 's as better guesses, return to step 2, repeat the process until further repetitions cease producing any significant changes in these values.

Step 6: These final values of T , p will satisfy energy and mass balance, and will be the steady-state result of the stack.

Step 7: Other related values of parameter can be calculated from them.

5.3 Unsteady State Models

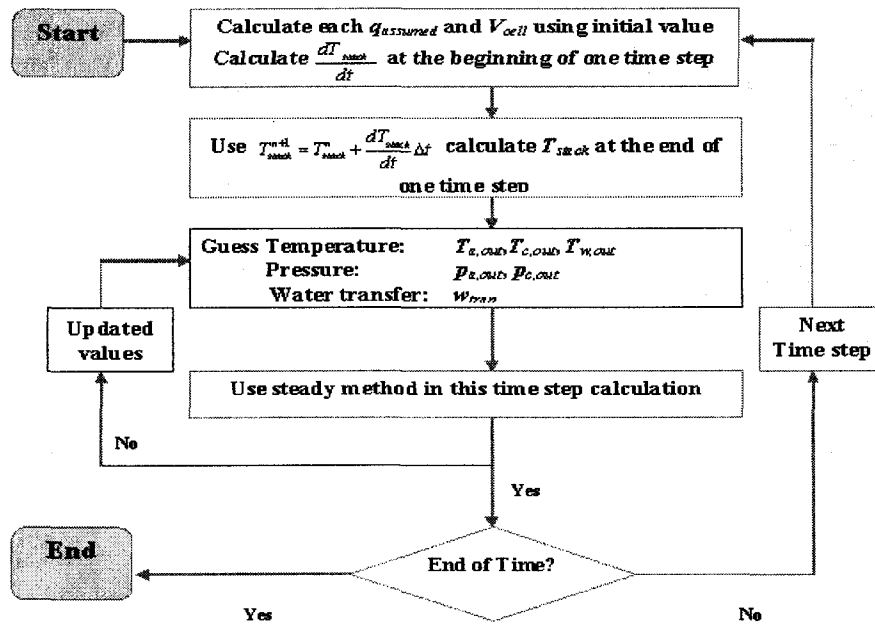


Fig. 16. Unsteady case calculation methodology

Parameters will change with the time in unsteady state. The time step $\Delta t = 1$ sec was used in the dynamic calculations, thus changes of all the parameters could be traced at each second.

Step 1: Calculate energy term and V_{cell} by initial input values. Use unsteady-state thermal model equation to get the value of dT_{stack}/dt at the beginning of the first time step.

Step 2: Calculate T_{stack} value at the end of the first time step, guess the value of $T_{w,out}$, $T_{a,out}$, $T_{c,out}$ and $p_{a,out}$, $p_{c,out}$.

Step 3: Keep fixed value of T_{stack} , follow steady state calculation steps to find all parameter values at the end of the first time step.

Step 4: For next time step, go to step 1, use those value got from Step 3 as the initial values, and repeat the process until reach the end of time period.

6. RESULTS AND DISCUSSIONS

6.1 Validation of the model

In the calculations presented here, unless specified otherwise, $RH = 1$ for both anode and cathode inlet stream. Table 4 shows the input data for the calculated case that was similar to the case reported by Amphlett *et al.* [36] and a comparison has been discussed by Yu and Zhou [37]. Table 5 lists the dimension values of fuel cell channel and stack used in our simulation. The land is the solid interval between the parallel channels.

Table 4. Inlet parameters of stack Ballard Mark V at 20A

Parameter	Value
$N_{H_2,a,in}$	0.0078 mol/s
$T_{a,in}$	23.5 °C
$P_{a,in}$	35 psig
$N_{O_2,c,in}$	0.004 mol/s
$T_{c,in}$	23.5 °C
$P_{c,in}$	35 psig
$N_{w,in}$	1.84 mol/s
$T_{w,in}$	23.5 °C
T_{room}	23.5 °C
k_{cell}	35 cells

Table 5. Stack and channels dimension table

Parameters	Width (mm)	Depth (mm)	Land (mm)	Number
Anode	1.25	0.8	1.0	5
Cathode	1.25	0.8	1.0	3
Coolant	2.5	0.8	4.0	5
Stack	Length/ Width/ Height:			0.38m/0.21m/0.21m

Model validation is conducted here by comparing our simulation results with the experimental results from two groups, which are listed in Table 6. First we compare our result with the testing data in [36], from case 1 in Table 6 we can see that we get the perfect match on cathode exit temperature, cooling water exit temperature, stack temperature and cell voltage output. However the anode exit temperature is quite different, our result of anode exit temperature is higher than in [36]. The error is due to the different content of anode gas. We try to simulate under the exact working condition as in [36], but we don't know the anode gas content they used in their testing. In our simulation, we use pure hydrogen gas, in [36] anode inlet includes carbon dioxide, and no its flow rate value available, because carbon dioxide exists, higher flow rate and higher specific heat will reduce anode stream temperature, that the reason why anode temperature in [36] is low than ours. There is a difference between stack temperatures, the testing result is higher than our simulation, we believe that this error is from we use the uniform stack temperature in our simulation, i.e., whole stack solid share the same temperature, it is reasonable that this value is lower than the testing value which is retrieved from thermocouple.

Comparison		Anode exit (°C)	Cathode exit (°C)	Cooling water (°C)	Stack solid (°C)	Voltage (V)	
1	I=20A	[36]	25.3	38.8	23.9	38	0.82
		This model	32.54	38.61	24.9	33.79	0.87
2	I=60A	[36]	–	–	–	60	0.73
		This model	–	–	–	53.3	0.81
3	I=79.1A Note 1	[33]	–	–	–	76	0.74
		This model	–	–	–	69.0	0.669
4	I=90.8A Note 2	[33]	–	–	–	68	0.71
		This model	–	–	–	77	0.61

Table 6. Result comparison with the experimental data($\varphi_{a,in} = \varphi_{c,in} = 1.0$).

Note 1. $p_{anode} = 45\text{psig}$, $p_{cathode} = 59\text{psig}$;

Note 2. $p_{anode} = 44\text{psig}$, $p_{cathode} = 37\text{psig}$;

In case 2, 3, 4, the published experimental data are available only on stack temperature and cell voltage in [33] and [36], from the comparison we see that our model can predict the stack performance well.

6.2 Steady cases

Fig. 17 shows temperature of the exits at anode, cathode, and water coolant with respect to the steady operating currents from 2A to 80A. It could be seen that all the temperatures increased with the increase of steady operating current and the cathode exit temperature was higher than the stack temperature, anode temperature and coolant temperature.

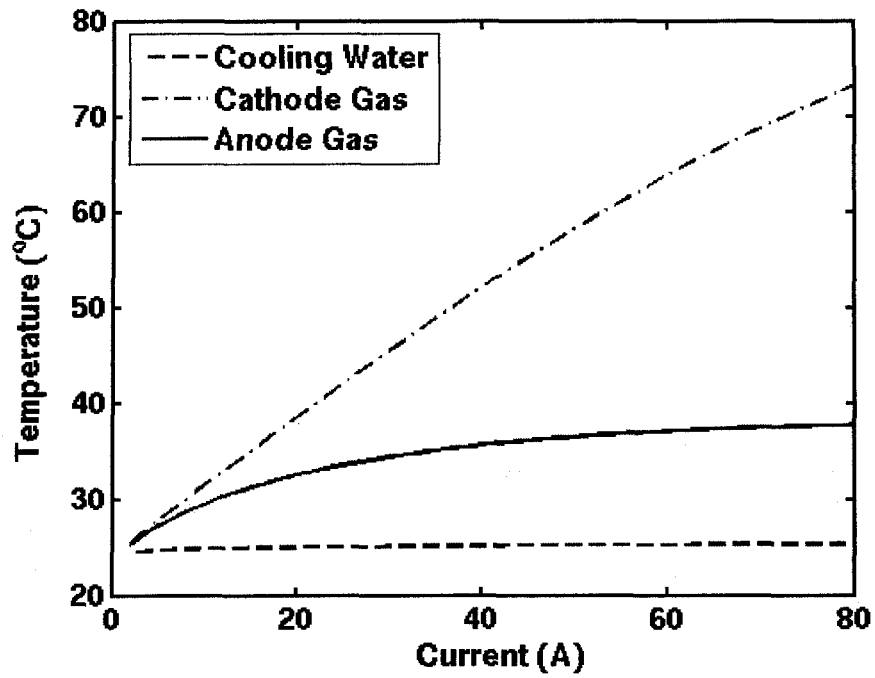


Fig. 17. Exit temperatures of flow streams with steady operating currents from 2 to 80A.

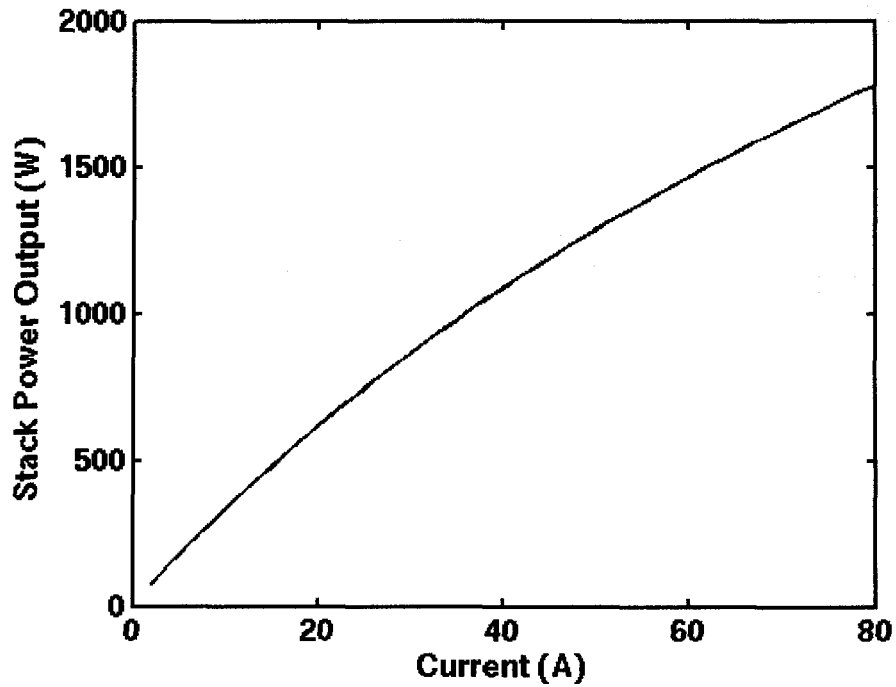


Fig. 18. Stack power output with steady operating current from 2 to 80A.

Fig. 18 is the output stack power at different steady operating currents from 2A to 80 A. The power output almost increased linearly with the steady operating current.

6.3 Steady cases with different ϕ value at inlet

In Fig. 19, the anode exit temperature at $\phi_{a,in} = 0.5, 1.0$ and 1.5 was plotted. Here $\phi_{a,in}$, relative water content at anode inlet, represents the molar ratio between total amount of supplied water (liquid + vapour) at anode inlet and the saturated water vapour carried by the anode inlet stream. When $\phi_{a,in} < 1$, the anode outlet temperature did not vary significantly with $\phi_{a,in}$. When $\phi_{a,in} > 1$, liquid water would mix with anode inlet stream and thus different $\phi_{a,in}$ values would have an obvious effect on anode outlet temperature, attributable to liquid water vapourization leading to anode exit temperature reduction. Basically, when inlet $\phi_{a,in}$ value increased, the anode exit temperature decreased.

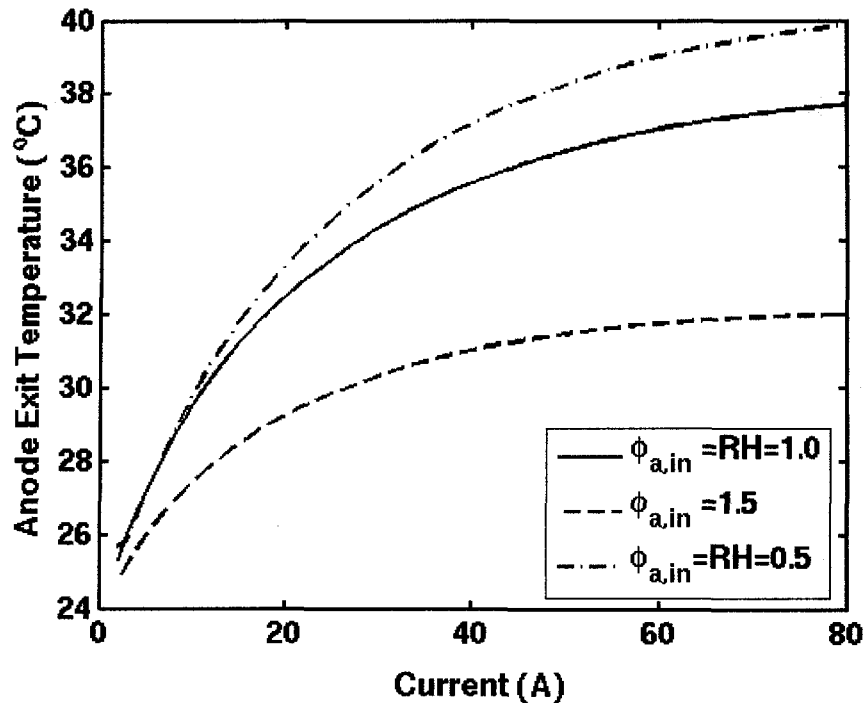


Fig. 19. Anode exit temperature at $\phi_{a.in}=0.5, 1.0$ and 1.5 .

Fig. 20 shows the stack temperature and voltage with different operating currents. Output voltage decreased when current was increased, attributable to a higher current creating a larger ohmic over-voltage loss.

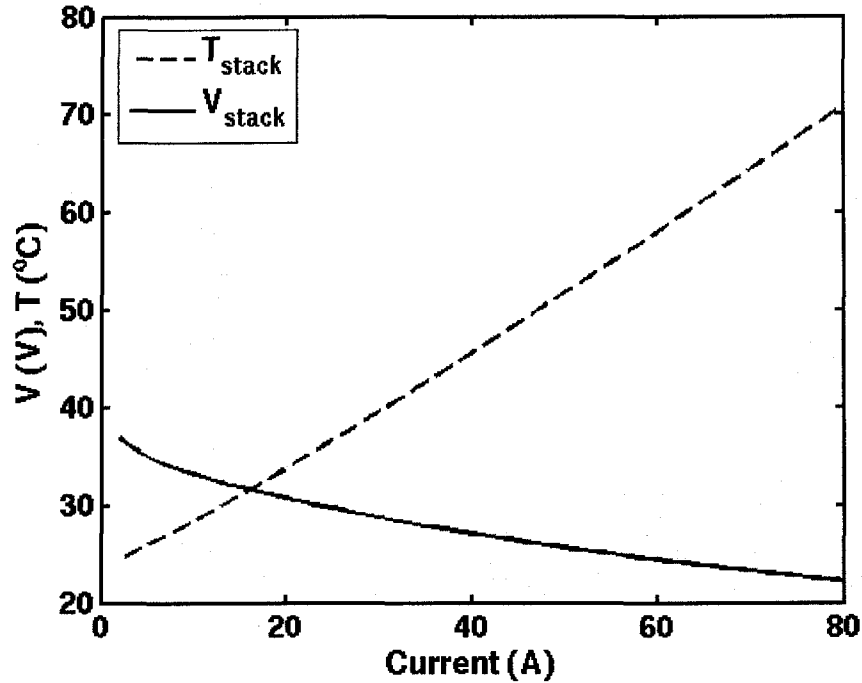


Fig. 20. Stack temperature and voltage at steady operating Current from 2 to 80 A

Fig. 21 shows stack voltage output at different $\phi_{a.in}$ for steady operating conditions. Electro-osmotic drag would be the dominant factor affecting the amount of water transferred across the membrane. Water was dragged from the anode to cathode side resulting in dry gas at the anode side which would reduce membrane conductivity and subsequently lower the stack voltage. Therefore, in order to achieve a higher voltage

output, extra humidification has to be provided to the gas at the anode side; It also could be seen in Fig. 21 that voltage output increased when the inlet $\phi_{a,in}$ was raised.

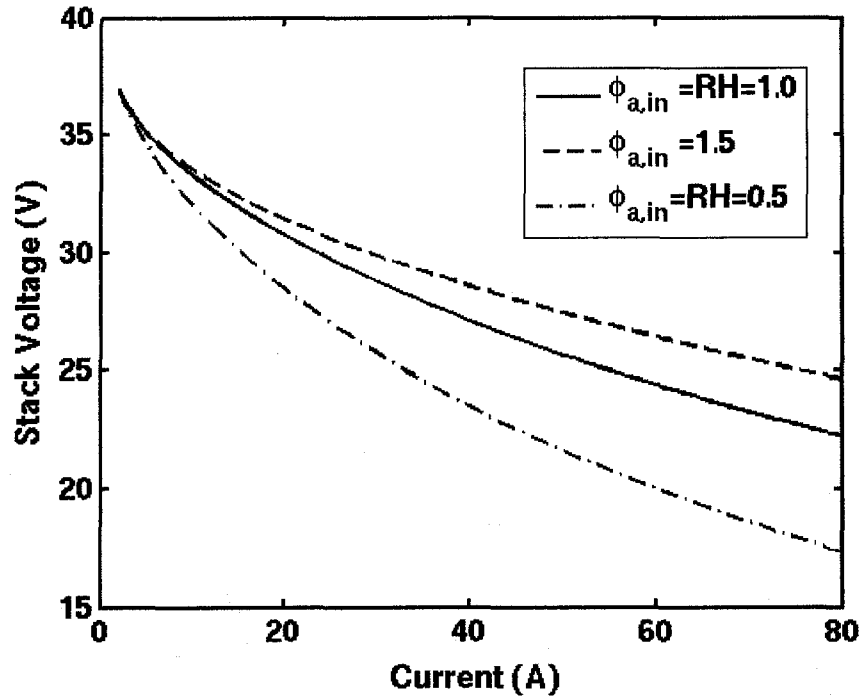


Fig. 21. Stack voltage with different $\phi_{a,in}$ at current from 2 to 80A

6.4 Unsteady Cases

Fig. 22 and Fig. 23 show the start-up characteristics of this stack at the operating current of 30 A; Fig. 22 shows the transient exit temperature plots while Fig. 23 shows the stack temperature and voltage.

From Fig. 22 and Fig. 23, it could be seen that the stack required about 30 to 40 minutes to reach steady state with the operating current of 30 A. In the first 20 minutes, the rate-of-exit temperature increase was high then slowly reduced until about 40 minutes when the stack almost reached its steady operating state.

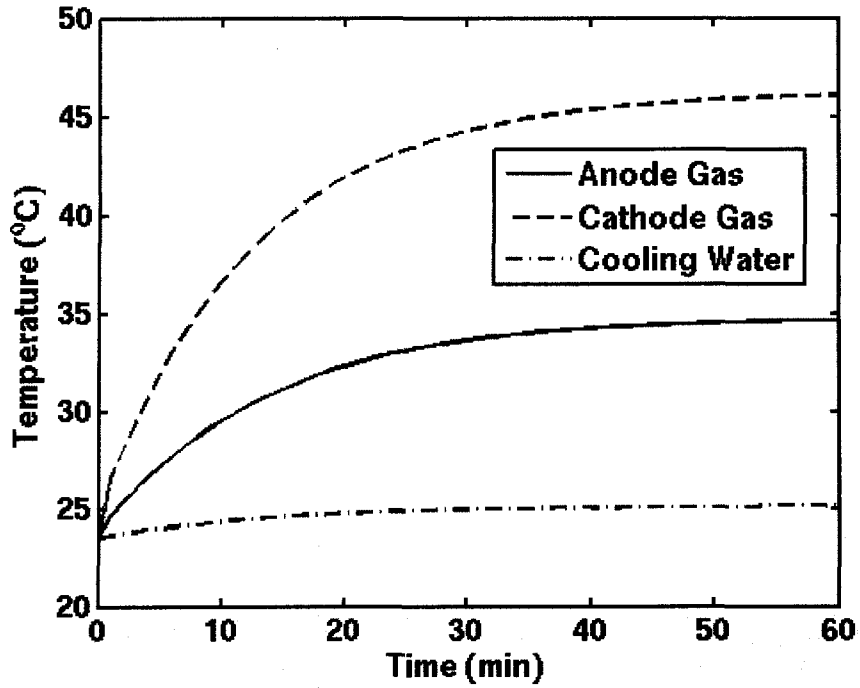


Fig. 22. Transient exit temperature plots of the start-up process for the operating current at 30 A.

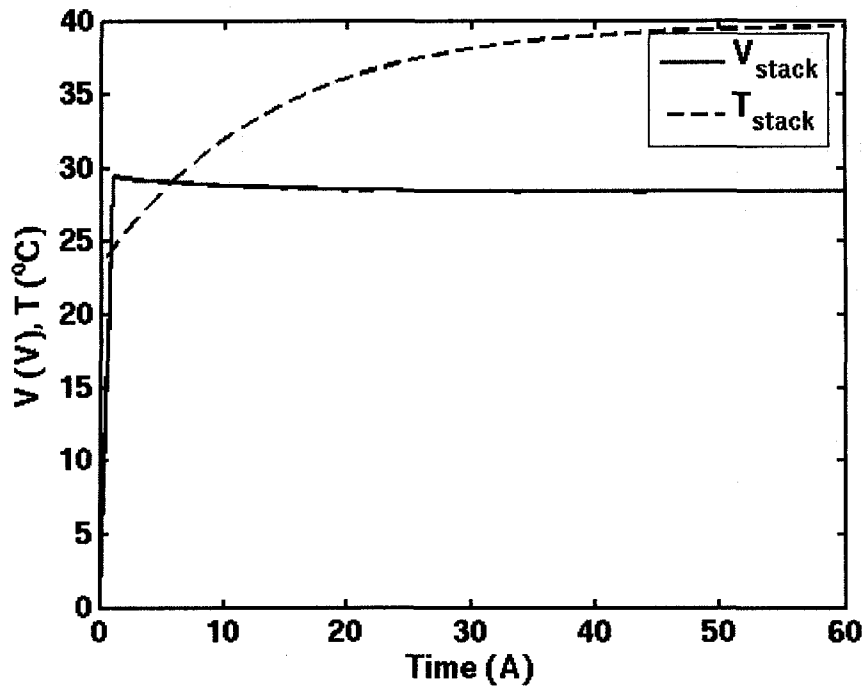


Fig. 23. Transient plot for the stack temperature and voltage of the start-up process for the operating current at 30 A.

The transient response of the stack for the load-set-up from 30 A (for 60 minutes) to 50 A (for another 60 minutes) are shown in Fig. 24 and Fig. 25. In general, the stack required about 40 minutes to reach its steady operating state after the load was changed. It is noteworthy that when the load was changed from 30 to 50 A, the immediate exit temperatures of anode and water coolant decreased because the amount of air and water with lower temperature increased from the inlets. Furthermore, from Fig. 25, the stack voltage at operating current of 50 A was lower than that at 30 A, due to the increase of current that would create larger over-voltages and thus smaller cell and stack voltage.

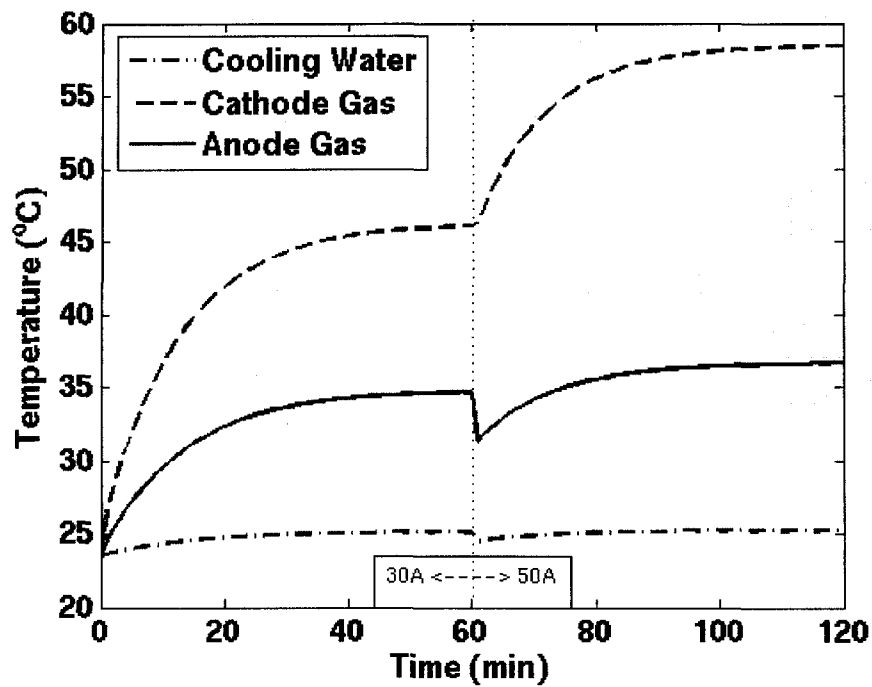


Fig. 24. Transient plot of flow streams coolant during the load set-up from 30 to 50 A.

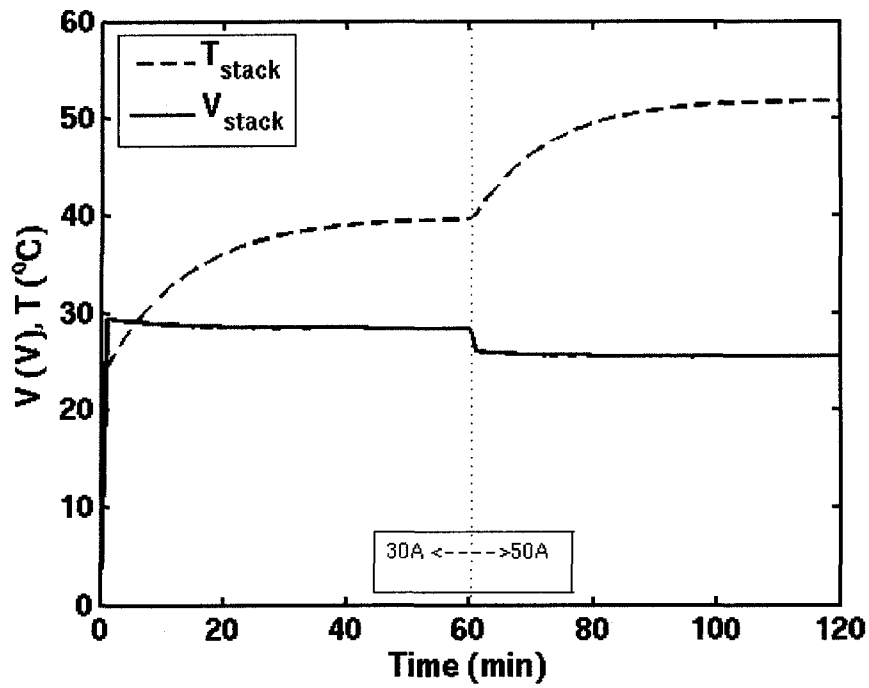


Fig. 25. Transient plot of stack temperature and voltage during the load set-up from 30 to 50 A.

Fig. 26 shows the temperature change in all streams as function of time and current change while Fig. 27 gives the stack voltage output and temperature change as function of time and load change. The load changed in each 20 minutes, from 20A to 40A, to 60A, to 40A, and to 20A within 100 minutes.

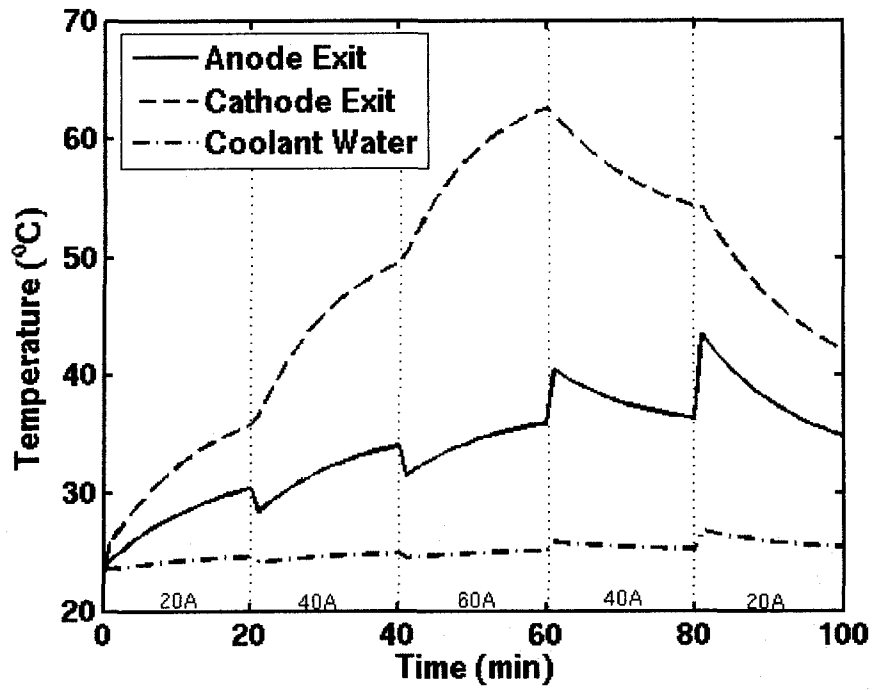


Fig. 26. Exit temperature change with time/load ($\phi_{a,in} = \phi_{c,in} = 1.0$).

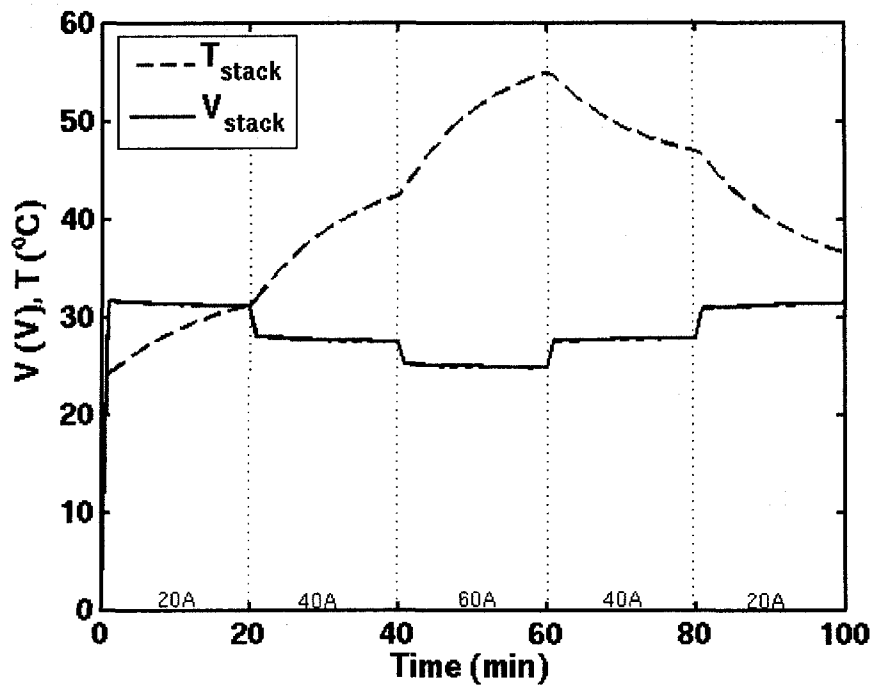


Fig. 27. Stack temperature and voltage change ($\phi_{a,in} = \phi_{c,in} = 1.0$).

Fig. 28 shows the values of stack voltage in terms of current change as a sine function $I = 50 + 20 \sin(t \cdot \pi / 30)$ where the stack current curve was plotted as a reference. During the current change from 30A to 70A, the voltage output slew in the range 22V to 28V and the minimum voltage output value was attained when the current (power output curve had the same pace) was at its maximum value due to voltage ohmic loss.

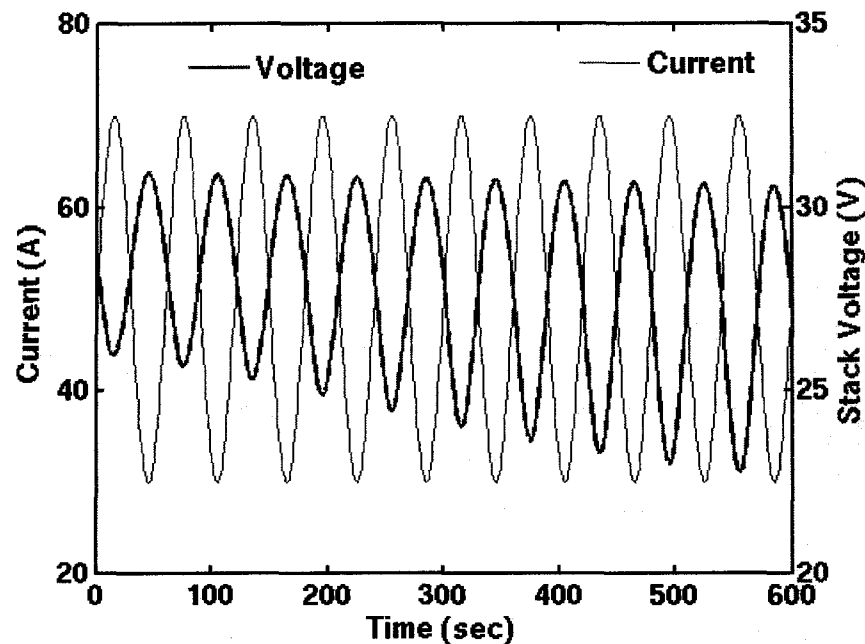


Fig. 28. Stack voltage as a function of current which changes with time as $I = 50 + 20 \sin(t\pi/30)$.

For the steady case, the average efficiency was around 45%~65%, depending on the voltage, energy loss to the surrounding and the stream sensible heat. For the unsteady case, when the current approached zero, the efficiency approached its peak value with the maximum attained at close-to 0A; the efficiency then quickly reduced as the current increased as observed in Fig. 29. When the current and power output had the same phase, therefore, when the current reached its peak in each period, the power output also reached its maximum value, however, stack efficiency had the opposite trend.

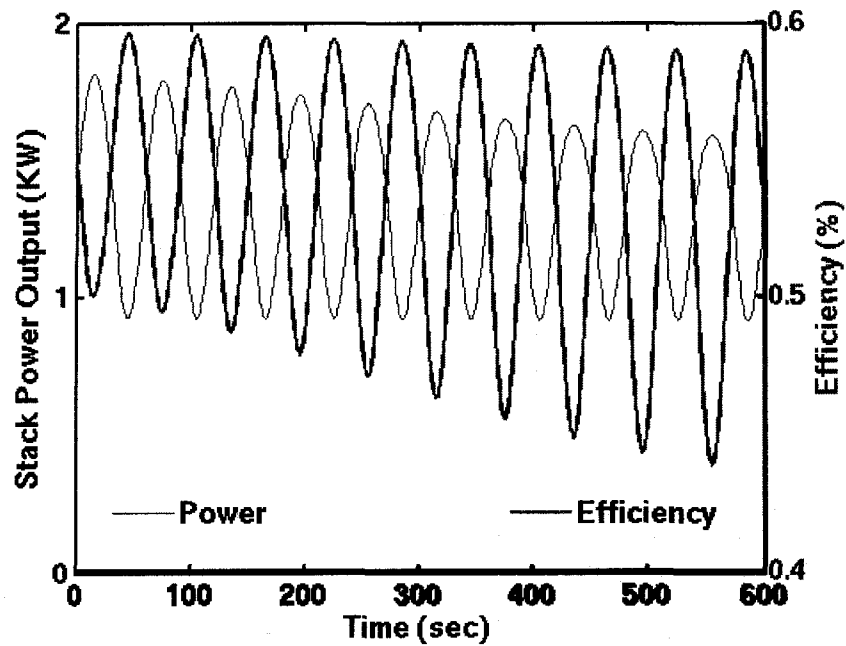


Fig. 29. Stack power output and efficiency as a function of current which changes with time as $I = 50 + 20 \sin(t\pi/30)$.

6.5 Water transportation

Water will transfer from anode side to cathode side by electro-osmotic drag flux. This flux is caused by hydrogen ion drag. When hydrogen ions go through membrane, each of them will carry some water molecule with them from anode to cathode. Because some amount transferred and no water products inside the channel, anode gas relative humidity will become lower and lower, dry anode gas will reduce membrane conductivity. The small geometry of anode channels won't allow too much liquid water mixed with inlet gas, besides cathode side water management, the proper design of anode channel will be very important to keep anode channel relative humidity at a reasonable range. Fig. 30 shows the water transfer amount during the operation with the current change from 2 to 80A. Basically, water transfer amount agrees with the working current because electro-osmotic drag is dominant.

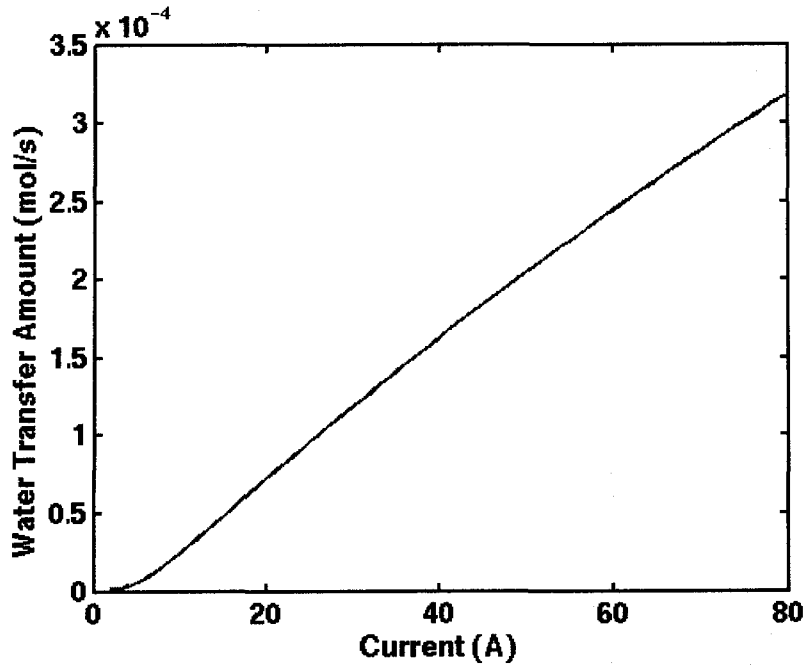


Fig. 30. Water transfer amount at the operating current from 2 to 80A.

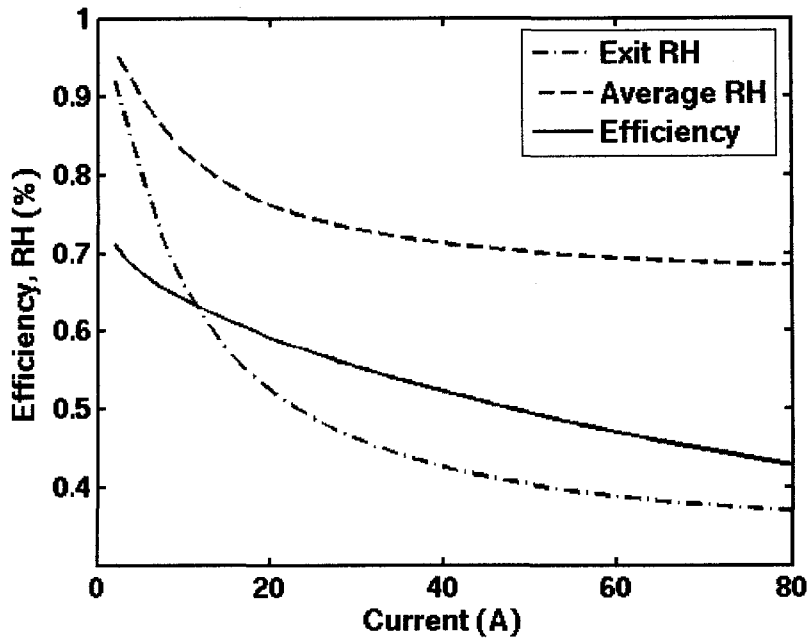


Fig. 31. Stack efficiency and anode average RH, exit RH at the operating current from 2 to 80A

Fig. 31 shows the values of anode stream average relative humidity and the relative humidity at exit during current change when from 2 to 80A at $\phi_{a,in}=1$. We can see that at

steady operating 80A, the exit RH is around 0.3, at this time, unreasonable stack efficiency will be observed when the working current is increased continually

6.6 System view of efficiency

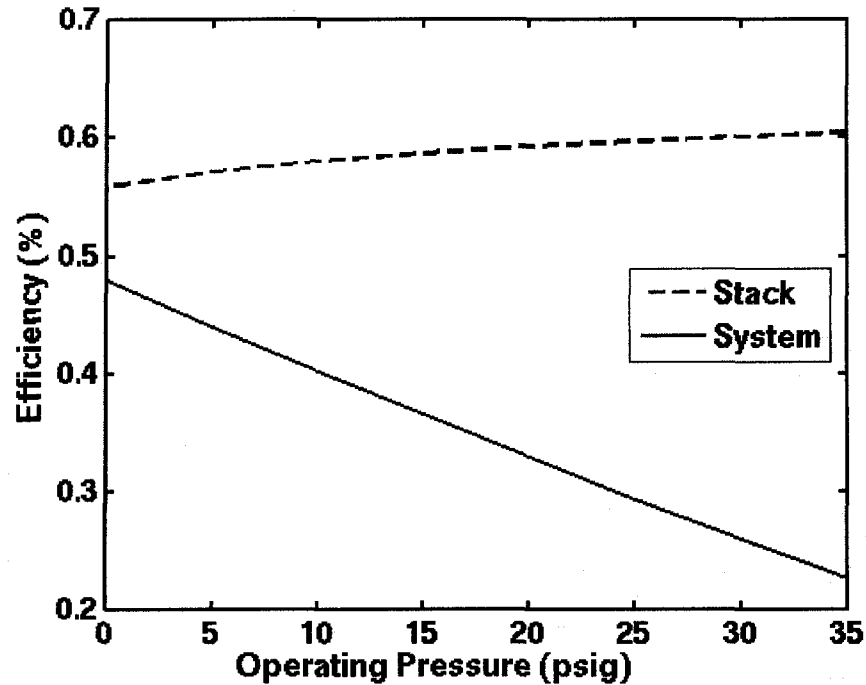


Fig. 32. Efficiency of fuel cell stack and system at different operating pressure ($I=20A$, $\phi_{a,in}=1$)

The two curves in Fig. 32 show the efficiency of stack operation when the pressure increased, the solid line presents the stack efficiency without considering the energy consumed by air compressor and water pump, the dashed line shows the system efficiency, the electrical powers consumed by pump and compressor have been deducted from the power generated from stack. From these two curves, we see that the benefit of higher operating pressure is less than the loss of consumed electrical power, the system efficiency becomes unacceptable when pressure is over 35psig. By giving sufficient

operating parameters, our model could do system optimization, and select the best working condition for the system.

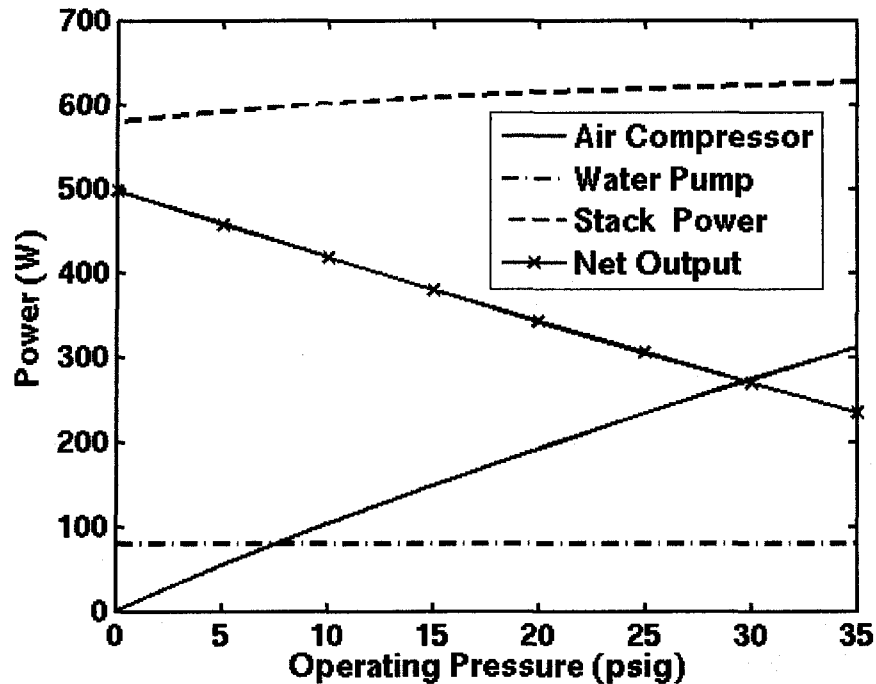


Fig. 33. Powers consumed and stack generated under different operating pressure ($I = 20A, \phi_{a,in}=1$)

Fig. 33 shows the compressor consumed power and the power generated by fuel cell stack under different operating pressure. We can see that as pressure increased, the electrical power consumed by compressor is growing faster than the rate of stack generated (for a fixed working current, the coolant flow rate is fixed here, so coolant pump consumed constant electrical power), as a result, the net power output of fuel cell system will reduce.

Fig. 34 is the same as the working condition in Fig. 32, the only difference is the anode inlet RH = 1.5 here. We can see that both stack efficiency and system efficiency are growing with the increased anode RH value, this is because the membrane will have a

higher conductivity than when anode RH = 1, stack power output is increased, and for RH = 1.5, the pumping power of extra inlet water vapour amount can be omitted

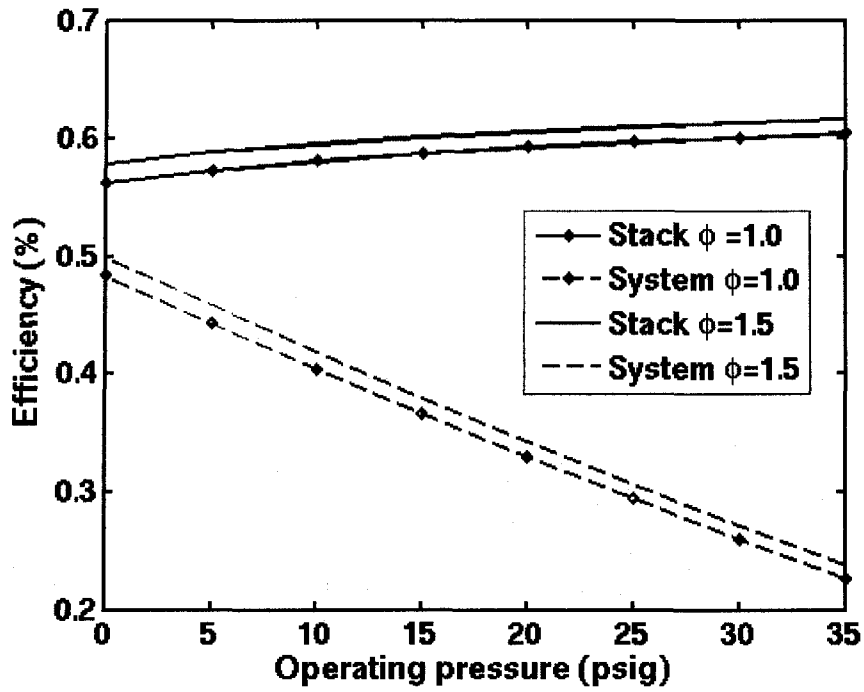


Fig. 34. Efficiency of fuel cell stack and system at different operating pressure
($I=20A$, $\phi_{a,in}=1.5$)

7. CONCLUSIONS AND RECOMMENDATION

Based on the simulation results using our simplified model on both steady and unsteady cases, we can draw some preliminary conclusions as follows.

1. Stack operating current and stack efficiency

1) When stack working current increases, the stack voltage will be reduced. As a result, stack efficiency will suffer.

2) There are two reasons to cause the low voltage value when current increases: the first is the ohmic loss in external electrical circuit; the second is the membrane conductivity becomes lower when the current increases.

3) For a fixed anode inlet RH value, the higher the current, the higher the water drag amount, the lower RH value on the anode side. The lower average RH value of the anode stream will make the membrane conductivity smaller.

4) The value of cathode channel relative water content ϕ is always bigger than unity, which means cathode stream is saturated all the time.

2. Stack operating pressure and system efficiency

Higher pressure can increase the stack efficiency, but it may not increase the system efficiency. This is because that although fuel cell stack can have more output power and higher efficiency at higher working pressure, the air compressor, at the same time, also consumes more electrical power.

3. Anode RH value and stack voltage

1) When uses extra humidification on the anode side, stack will achieve higher voltage output. But to avoid liquid water block the channels, we have the limitation on the inlet water liquid amount.

2) The PEM fuel cell stack studied in this work takes about 30 to 40 minutes to reach its steady operation after start up.

4. Recommendation and future work

The present work is a preliminary attempt to model PEM stack. The model presented here should be validated through systematic experimental investigation.

References

- [1] J. Larminie, A. Dicks, Fuel Cell Systems Explained, John Wiley & Sons, Ltd, 2002.
- [2] T. Yokoyama, Y. Naganuma, K. Kuriyama, M. Arimoto, Development of Fuel-Cell Bus, SAE Paper 01 (2003) 04-17.
- [3] J.K. Seong, O.B. Soo, Fuel Economy and Life-Cycle Cost Analysis of a Fuel Cell Hybrid Vehicle, Journal of Power Sources 105 (2002) 58–65.
- [4] M. Ogburn, D.J. Nelson, W. Luttrell, B. King, S. Postle, R. Fahrenkrog, Systems Integration and Performance Issues in a Fuel Cell Hybrid Electric Vehicle, SAE Paper 01 (2000) 03-76.
- [5] J.M. Ogden, M.M. Steinbugler, T.G. Kreutz, A Comparison of Hydrogen, methanol and gasoline as Fuels for Fuel Cell Vehicles: implications for vehicle design and infrastructure development. Journal of Power Sources, 79-2 (1999) 143–168.
- [6] E. Per, R. Monika, The Fuel Cell Vehicle Analysis of Energy Use, emissions and cost. International Journal of Hydrogen Energy, 23-5 (1998) 381–385.
- [7] Y.J. Zhang, M.G. Ouyang, J.X. Luo, Z. Zhang, Y.J. Wang. Mathematical modeling of Vehicle Fuel Cell Power System Thermal Management, SAE Paper, 01 (2003) 11-46.
- [8] R. Andrew, X.G. Li, Mathematical Modeling of Proton Exchange Membrane Fuel Cells, Journal of Power Sources, 102 (2001) 82–96.
- [9] Transportation Fuel Cell Power Systems Annual Progress Report, US. Department of Energy, December 2001.
- [10] Transportation Fuel Cell Power Systems Annual Progress Report, US. Department of Energy, October 2000.

- [11] M. Nadal, F. Barbir, Development of a Hybrid Fuel Cell/Battery Powered Electric Vehicle, *International Journal of Hydrogen Energy*, 21 (1996) 497–505.
- [12] J.C. Amphlett, R.M. Baumert, R.F. Mann, B.A. Peppley, P.R. Roberge, Parametric Modeling of the Performance of a 5-kW Proton Exchange Membrane Fuel Cell Stack, *Journal of Power Sources*, 49 (1994) 349–356.
- [13] W.R. Dunbar, R.A. Gaggioli, Computer Simulation of Solid Electrolyte Fuel Cells. *Journal of Energy Resources Technology*, 112 (1990) 1-14.
- [14] T.E. Springer, T.A. Zawodzinski, S. Gottesfeld. Polymer Electrolyte Fuel Cell Model, *J. Electrochem. Soc.*, 138-8 (1991) 2334-2342.
- [15] M.W. Verbrugge, R.F.Hill. Transport Phenomena in Perfluorosulfonic Acid Membranes During the Passage of Current, *J. Electrochem. Soc.* 137-4 (1990) 1131-1138.
- [16] D.M. Bernardi, M.W. Verbrugge, Mathematical Model of a Gas Diffusion Electrode Bonded to a Polymer Electrolyte, *AICHE J.*, 37-8 (1991) 1151-1163.
- [17] D.M. Bernardi, M.W. Verbrugge, A Mathematical Model of the Solid-Polymer-Electrolyte Fuel Cell, *J. Electrochem. Soc.*, 139-9 (1992) 2477-2491.
- [18] T.F. Fuller, J. Newman, Water and Thermal Management in Solid-Polymer-Electrolyte Fuel Cells, *J. Electrochem. Soc.*, 140-5 (1993) 1218-1225.
- [19] T.V. Nguyen, R.E. White, A Water and Heat Management Model for Proton-Exchange-Membrane Fuel Cells, *J. Electrochem. Soc.*, 140-8 (1993) 2178-2186.
- [20] J. Kim, S. Srinivasan, C.E. Chamberlin, Modeling of Proton Exchange Membrane Fuel Cell Performance with an Empirical Equation, *J. Electrochem. Soc.*, 142-8 (1993) 2670.

- [21] T. Berning, D.M. Lu, N. Djilali, Three-Dimensional Analysis of Transport Phenomena in a PEM Fuel Cell, *Journal of Power Sources*, 106 (2002) 284-294.
- [22] A. Rowe, X. Li, Mathematical Modeling of Proton Exchange Membrane Fuel Cells, *Journal of Power Sources*, 102 (2001) 82-96.
- [23] J.J. Baschuk, X. Li, Modeling of Polymer Electrolyte Membrane Fuel Cells with Variable Degrees of Water Flooding, *Journal of Power Sources*, 86 (2000) 181-196.
- [24] C. Marr, X. Li, Composition and Performance Modeling of Catalyst Layer in a Proton Exchange Membrane Fuel Cell, *Journal of Power Sources*, 77 (1999) 17-27.
- [25] D. Xue, Z. Dong, Optimal Fuel Cell System Design Considering Functional Performance and Production Costs, *Journal of Power Sources*, 76 (1998) 69-80.
- [26] P. Costamagna, S. Srinivasa, Quantum Jumps in the PEMFC Science and Technology from the 1960s to the year 2000 Part II. Engineering, Technology Development and Application Aspects, *Journal of Power Sources*, 102 (2001) 253-269.
- [27] J.H. Lee, T.R. Lark, A.J. Appleby, Modeling Electrochemical Performance in Large Scale Proton Exchange Membrane Fuel Cell Stacks, *Journal of Power Sources*, 70 (1998) 258-268.
- [28] J.H. Lee, T.R. Lark, Modeling Fuel Cell Stack Systems, *Journal of Power Sources*, 73 (1998) 229-241.
- [29] N. Djilali, D.M. Lu, Influence of Heat Transfer on gas and Water Transport in fuel cells, *International Journal of Thermal Sciences*, 41 (2002) 29–40.
- [30] N.S. Ap, Influence of Front End Vehicle, Fan and Fan Shroud on the Cooling System of Fuel Cell Electric Vehicle (FCEV), *EVS 18*, Berlin, 2001.

- [31] M.H. Fronk, D.L. Wetter, D.A. Masten, A. Bosco, PEM Fuel Cell System Solutions for Transportation, SAE Paper, 01 (2000) 0373.
- [32] G. Maggio, V. Recupero, C. Mantegazza, Modeling of Temperature Distribution in a Solid Polymer Electrolyte Fuel Cell Stack, Journal of Power Sources, 62 (1996) 167–174.
- [33] J.C. Amphlett, R.M. Baumert, R.F. Mann, B.A. Peppley, P.R. Roberge, A. Rodrigues, Parametric Modeling of the Performance of a 5-kW Proton Exchange Membrane Fuel Cell Stack, Journal of Power Sources, 49 (1994) 349-356.
- [34] J.C. Amphlett, R.M. Baumert, R.F. Mann, B.A. Peppley, P.R. Roberge, T.J. Harris, Performance Modeling of the Ballard Mark IV Solid Polymer Electrolyte Fuel Cell: II Empirical Model Development, J. Electrochem. Soc., 142 (1995) 9-15.
- [35] J.C. Amphlett, R.M. Naumert, R.F. Mann, B.A. Peppley, P.R. Roberge, T.J. Harris, Performance Modeling of the Ballard Mark IV Solid Polymer Electrolyte Fuel Cell: I Mechanistic Model Development, J. Electrochem. Soc., 142 (1995) 1-8.
- [36] J.C. Amphlett, R.F. Mann, B.A. Peppley, P.R. Roberge, A. Rodrigues, A model Predicting Transient Response of Proton Exchange Membrane Fuel Cells, Journal of Power Sources, 61 (1996) 183-188.
- [37] Xiaochen Yu, Biao Zhou, Steady and Unsteady Modeling of Ballard Mark V PEM Fuel Cell Stack, CSME Forum S7 (2004) 1091-1100.
- [38] B.R. Munson, D.F. Young, T.H. Okiishi, Fundamentals of Fluid Mechanics, 4th Edition, (2002) pp475.
- [39] Shan-Hai Ge, Bao-Lian Yi, A Mathematical Model for PEMFC in Different Flow Modes, Journal of Power Sources 124 (2003) 1–11.

- [40] Yemada Taitel , A.E.Dukler, A Model for Predicting Flow Regime Transitions in Horizontal and Near Horizontal Gas-Liquid Flow, *AICh E Journal*, 22(1976) 47-54.
- [41] Klaus Tüber, David Pócza and Christopher Hebling, Visualization of Water Buildup in the Cathode of a Transparent PEM Fuel Cell, *Journal of Power Sources*, 124(2003) 403- 414.
- [42] G. Hetsronia, D. Mewesb, C. Enkeb, M. Gurevicha, A. Mosyaka, R. Rozenblita, Heat Transfer to Two-Phase Flow in Inclined Tubes, *International Journal of Multiphase Flow*, 29(2003) 173-194.
- [43] Fujita. H. Ohara, T. Hirota, M. Furuta, H., Gas–Liquid Flows in Flat Channels with Small Channel Clearance, *Proceedings of the Second International Conference on Multiphase Flow '95, Kyoto, Japan*, IA3-37–IA3-44.
- [44] Ide. H. and Matsumura, H., Frictional Pressure Drops of Two-Phase Gas–Liquid Flow in Rectangular Channel, *Experimental Thermal Fluid Science*, 3(1990) 362–372.
- [45] Lowry, B. and Kawaji, M., Adiabatic Vertical Two-Phase Flow in Narrow Flow Channels, *AIChE Symposium Series*, 84 (1988) 263 133–139.
- [46] Mishima, K., Hibiki, T. and Nishihara, H., Some Characteristics of Air-Water Two-Phase Flow in Small Vertical Tubes, *International Journal of Multiphase Flow* , 22(1996) 703-712..
- [47] Han Ju Lee and Sang Yong Lee, Pressure Drop Correlations for Two-Phase Flow within Horizontal Rectangular Channels with Small Heights, *International journal of Multiphase Flow* 27(2001) 783-796.
- [48] SuperchargerOnline, Root Type Superchargers Explained, Aug 2005.

<http://www.superchargersonline.com>.

[49] <http://www.machinerylubrication.com>, Aug 2005.

[50] Nuclear Power Fundamentals, Aug 2005. <http://www.tpub.com>.

[51] Glenn Research Center, Aug 2005. <http://www.grc.nasa.gov>.

[52] Engineered Machined Products, Inc, Aug 2005. <http://www.emp-corp.com>.

[53] Bruce R. Munson, Donald F. Young, Theodore H. Okiishi, Fundamentals of Fluid Mechanics 4th, John wiley & Sons, Inc. 2002.

[54] Online chemical Information, Aug 2005.

<http://www.cheresources.com/centrifugalpumps5.shtml>

VITA AUCTORIS

NAME: Xiaochen Yu

PLACE OF BIRTH Harbin China

YEAR OF BIRTH 1970

EDUCATION HIT, Harbin China
1987-1991 B.Sc.
York University, Toronto, Ontario
2001-2003 BA
University of Windsor, Windsor, Ontario
2003-2005 M. Sc.